KU LEUVEN

Universidad Carlos III de Madrid

KU Leuven. Erasmus Stage/ Universidad Carlos III de Madrid

PFC: AlSi10Mg parts produced by Selective Laser Melting (SLM)

Promoter: Jan Van Humbeeck

Tutor: Lore Thijs

Miguel Godino Martínez . Industrial Engineering. Specialty: Materials
Leuven, (Belgium)31/05/2013

Index

Annex 1:Figures Index

Annex 2:Tables Index

1. 1. Abstract

Selective Laser Melting (SLM) is an Additive Manufacturing technique, which allows the production of parts starting from powder, using a laser beam and the aid of CAD computer techniques. Due to the layer wise production, complex geometrical pieces can be built achieving very good dimensional tolerances and high quality parts related to the mechanical properties.

The goal of this thesis is to study the microstructure and the mechanical properties of AlSi10Mg parts produced by SLM, depending on the SLM scanning parameters and the influence of aging treatments.

Moreover, a comparison between the traditional casting parts and SLM parts is done. For studying the properties, different microstructure analysis, density measurements, tensile test, hardness test, SEM and X-Ray diffraction tests are going to be developed and analyzed. Also, the effects of an aging treatment on AlSi10Mg parts will be discussed.

2. State of the art

This review is focused on the AlSi10Mg properties and manufacturing techniques. First, the material composition and properties are analyzed. Both casting and SLM manufacturing techniques are reviewed. Then the SLM process, parameters and scanning strategies are described with more detail. Finally, the influence of aging on SLM produced parts is given.

2.1. Properties

AlSi10Mg is a widely used alloy, characterized by its high corrosion resistance and low density, compared with other alloys. It has good weldability, good castability, hardenability and good static and dynamic resistance. The thermal conductivity is very high.

The composition of this alloy can be seen in the Table 1. The addition of silicon to the aluminium improves the creep and the corrosion resistance, and the addition of Mg allows the hardening of the alloy by forming precipitates (Mg_2Si), through aging treatments. The maximum useful limit of Mg for hardening corresponds to 0.7% Mg, while the normal range is 0.40-0.60 %. The addition of Mg above 0.7% can contribute to the softening of the matrix. [ASM92]

Table 1 Composition of AlSi10Mg parts (wt %)[ASM92]

AlSi10Mg	UNS A03600	Si 9.0 - 10.0 Mg 0.40 - 0.6 Mn 0.35 Ni 0.5 Al 85.7-86.6	Cu 0.03 Fe 2.0 Ti 0.15 Zn 0.50 Sn 0.15

Due to the combination of light weight, high heat conductivity and good mechanical properties, it is suitable for the aerospace industry, as well as the automotive. The overview of properties is resumed in Table 2 .

AlSi10Mg alloys are light density alloys, as one can see if one compares the density of AlSi10Mg alloys(2,68g/cm^3) with others materials, as pure iron (7.874 g/cm^3). Related to the thermal conductivity, its value is 160W/m.K, while materials as carbon steels has around 54W/m.K, and others as the higher thermal conductivity materials as Cupper shows a thermal conductivity of 401 W/m.K. The coefficient of thermal expansion is 20,5.10 $^{-6}$°C^{-1}, while for other materials is 25. 10 $^{-6}$ °C^{-1}(magnesium), 13.10 $^{-6}$ °C^{-1} (Nickel), 12.10 $^{-6}$°C $^{-1}$ (pure iron) or 46.10 $^{-6}$°C^{-1}(Lithium).

Table 2 Properties of AlSi10Mg [Adial.fr]

Properties	Value
Density (g/cm^3)	2.68
Solidification interval (K)	873-828
Thermal conductivity (W/m. K)	160
Resistivity (µΩ cm) at 20°C	4.5
Coefficient of thermal expansion (°C -1) (between 20°C and 100°C)	20,5.10 $^{-6}$

The good weldability allows not only producing AlSi10Mg by casting but also by Selective Laser Melting, due to the near-eutectic composition of Al and Si, which lowers the melting point as can be seen in Figure 1.

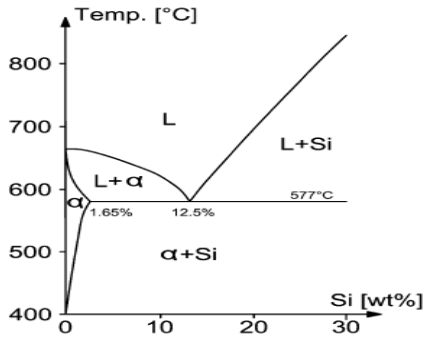

Figure 1 Al Si Phase diagram [BRA12]

The mechanical properties of SLM parts, such as elongation to fracture or hardness, are better than those of traditional casting ones without the need for thermal treatments. In Table 3 the mechanical properties of AlSi10Mg parts after traditional processing are shown.

Table 3 Mechanical properties of AlSi10Mg parts after traditional processing [KEM12]

x ± s	E(GPa)	UTS(MPa)	ε_{break} (%)	HV
Conventional cast and aged	71	300-317	2.5-3.5	86
High pressure die casting	71	300-350	3-5	95-105
High pressure die casting and aged	71	330-365	3-5	130-133

2.2. Production of Al alloys by casting.

The primary aluminium production is based on the Hall-Heroult process. Bauxite (65% alumina) is dissolved in a cryolited bath containing salts, and then, due to a electrical voltage, alumina is electrolyzed and the aluminium is obtained in the cathode.[ASM92] Although there are other ways of developing aluminium products, this review is focussing on the casting, which is the most common production technique for AlMg10Si alloys, and in additive manufacturing.(A M). In A M, which is the topic of this thesis, the material is also fully (completely melted). Aluminium can be processed by other techniques such as extrusion, forging and rolling.

Aluminium alloys can be casted by pressure die, permanent mould, plaster casting, or dry sand casting [ASM92].

In casting, the final grain size is one of the most important parameters to take into account. The grain size will determine the mechanical properties of the part. Very fine grains allow obtaining good properties, while coarse grains leads to worse mechanical properties. [TOT03].

For achieving finest grains in casting, modification methods are used, normally based on small amounts of special master alloys into an overheated melt, which modify surface properties, the particle size distribution, intermetallic morphology or processing parameters such as cooling rate, temperature or time[TOT03].

For Al-Si alloys, which is the topic of this thesis, the morphology and the distribution of the silicon crystals is a key factor in the final grain size of the alloy. Primary silicon crystals can be present in the melt until 800-1200 °C, so modifiers must act on these crystals. [TOT03]

Regarding to final shape consideration, different moulds can be used. The dimensional tolerance range desired is another factor to take into account when choosing the mould. In die casting, the dimensional tolerances for aluminium are +/- 0.10mm for basic tolerance (up to 25 mm length) and additional tolerances of +/- 0.04mm over 25mm to 300mm length and +/- 0.03 over 300mm length.[KAY09]

High pressure die casting usually allows obtaining the best mechanical properties amongst the casting methods. By die casting, molten material is introduced under pressure into the mould. There are two basic types of die casting machines: hot-chamber machines and cold-chamber machines. Most die casting is made from non-ferrous metals. This process is expensive, so is suitable for parts that need high quality, especially for achieving high dimensional tolerances, or for high volume production. (Scale economies).

2.3. SLM process.

Selective Laser Melting is an Additive Manufacturing technique. By Selective Laser Melting, the pieces are built layer by layer, melting layers of metal powder using the thermal energy provided by a laser beam. The system consists of a laser beam, scanner mirrors which deflect the laser, a powder scraper, a feed container, a base plate and a building platform, as one can see in Figure 2. The mirrors of the machine deflect the laser beam, guiding the movement of the laser over the surface of the powder bed. The powder heats up and melts when the laser beam irradiates. Selective laser melting

includes different heat transfer mechanisms, phase transformation, fluid flow in the molten pool due to surface-tension gradient and convection, evaporation and chemical reactions. There are models to study the SLM process taking into account also the effect of the evaporation that occurs in the SLM process, as described in [VER09] in which four

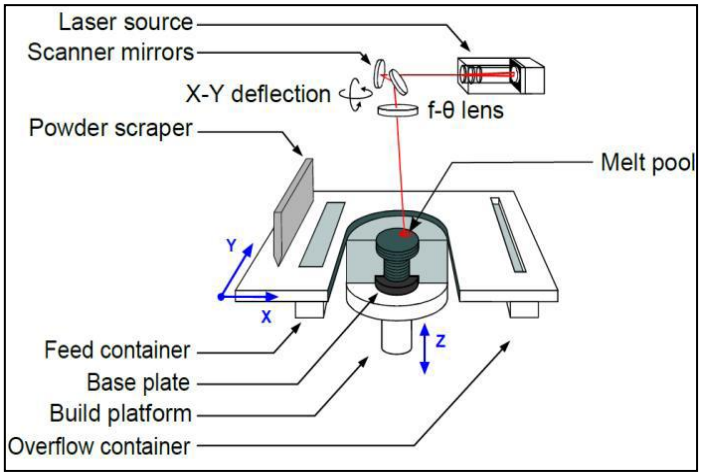

Figure 2 Schematic figure of the parts of a SLM machine [KEM12]

phases are taken into account: solid, liquid, vapor and pseudo phase powder phase.

By SLM complex geometry pieces can be built, based on 3D CAD data computer techniques. The SLM works in inert atmospheres, i.e. Argon atmosphere in order to handle with reactive materials. In this way, for AlSi10Mg one can achieve better mechanical properties by SLM than by methods such as traditional casting.

2.3.1. SLM parameters

SLM provides the possibility of obtaining different types of texture and different properties depending on the material, the way of scanning and the rotation of scanning. The laser beam melts the powder, creating tracks with a half pipe form. Several layers are deposited one after the other in the building direction when producing the piece. The scan strategy, together with the parameters of the laser, such

as scan velocity, power or scan distance between tracks are very important in order to obtain a high density and good mechanical properties of the pieces.

2.3.2.Power, scan velocity and distance between tracks

According to [KEM11] there is a relation between the density of the parts and the power. Scan speed, power of the laser, scan spacing and layer thickness are also both related; with the optimization of these four parameters one can achieve the optimal energy input for obtaining the highest density for the parts. The surface roughness is also related to the process parameters. The quality of the surface will be improved when melt pool tracks are more stable. The solidification mode and the fineness of the microstructure achieved with SLM are related to the gradient of thermal energy. It is shown that due to high thermal gradients very fine microstructures can be obtained. In general, the fineness of the cells along the melt pool is reduced in the centre of the tracks.

2.3.3. Scan strategy [THI12]

Depending of rotation and scanning, specific microstructures and textures will appear. One can consider 5 main ways of scanning strategies [THI12], as appears in the figure below. However, other different strategies can be applied as well.

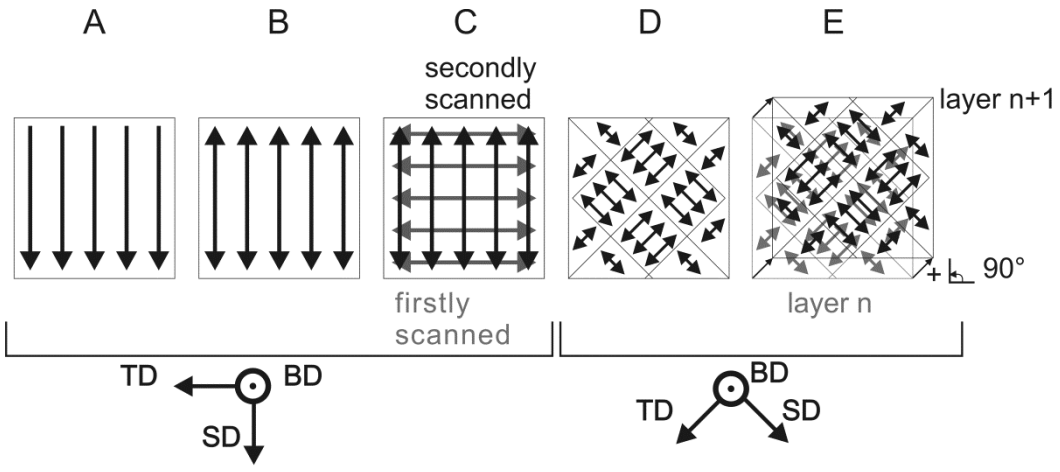

Figure 3 Scan strategies for producing SLM parts. The vectors indicate the direction and displacement of the laser beam. [THI12]

A. Unidirectional, no rotation.
B. Bidirectional, no rotation
C. Remelting 90° rotation between layers.
D. Island bidirectional scanning with 90° rotation.
E. Island bidirectional scanning with 90° rotation shifted.

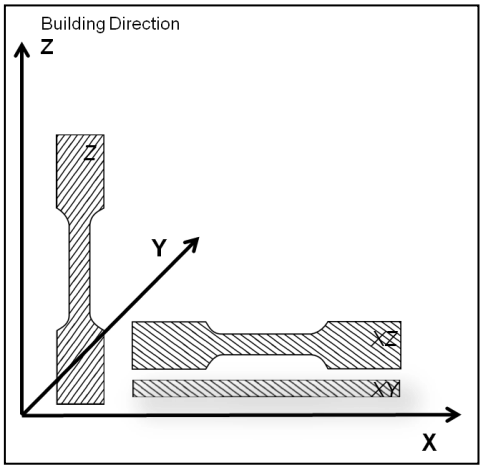

Figure 4. Schematic figure of the building orientation of the parts produced by SLM [KEM11]

2.3.3.1. Unidirectional and bidirectional strategies with no rotation.

In this strategy each layer is scanned one time, and all in the same direction. The results show that when there is no rotation between the layers, there is a strong preference for <100> crystal orientation in the direction of the scanning. [THI12] Some oxides and pores near the borders can appear. For bidirectional scanning strategy one can see a very fine cellular dentritic solidification structure, with three different zones: melt pool fine, melt pool coarse and the Heat Affected Zone (HAZ). So, when the heat flow coincides with the <100> direction one can observe epitaxial growth of grains, but if this does not happen, competitive growth appears that comes towards the heat flow

direction [THI12]. One can see a fine microstructure due to the cooling rate, with a fine Si distribution. Related to the texture, it is shown that the unidirectional or bidirectional way of scanning does not affect the texture in a significant way. [THI12]

2.3.3.2. Remelting between layers

This scanning strategy allows reducing the porosity much more than without remelting techniques. First, one layer is scanned in one direction, and afterwards, the same layer is scanned again with a rotation of 90°, so remelting takes place. However, the size of the second scanned melt pool is smaller than the first one.[THI12]

When rotating 90 ° between layers, a weaker cube structure in the building direction appears. The crystallographic texture is reduced when rotating between layers.

2.3.3.3. Island scanning

Island scanning, is done by dividing the cross section into islands, in order to divide the vector length. According to previous studies, the texture is also more reduced than when rotation is applied.

2.4. Mechanical properties, anysotropy and heat treatments.

Establishing a comparison between the mechanical properties of AlSi10Mg produced by SLM and High Die Pressure Casting, one can see that in general, mechanical properties obtained by SLM are better than traditional casting ones. This can be seen in Table 4

Table 4 Mechanical properties of AlSI10Mg parts produced by casting and SLM [KEM12]

	E(GPa)	UTS(MPa)	Elongation to break(%)	HV
SLM. XY direction	68 ± 3	391 ± 6	5,55 ± 0,4	127
SLM. Z direction		396 ± 8	3,47 ± 0,6	
HPDC	71	300-350	3-5	95-105
HPDC and aged	71	330-365	3-5	130-133

However, SLM pieces presents anisotropy, depending on the building direction. For Z building direction, tracks are shorter and more defects are created in the beginning and ending of the tracks, causing a decrease in the mechanical properties. [KEM12] Related with this, a higher porosity can be seen with more intensity at those zones for all the scanning strategies, due to the heat accumulated at these points. In this way, a keyhole is created, and due to less stability, the pores and defects will appear in these places; other kind of pores and oxides can also be seen [THI12].

2.4.1.Heat Treatment

A thermal treatment is usually needed after casting of aluminum in order to harden the piece by the precipitation of Mg_2Si

By SLM a very fine microstructure can be directly achieved, with a fine distribution of the Si, leading to very good mechanical properties.[KEM12] This happens due to the high energy and the rapid cooling rate that takes place using the laser beam melting. In this way SLM provides better mechanical properties compared with the traditional

casting parts, without aging them. [KEM12]. However, heat treatments for SLM pieces can also be done afterwards.

3. Experimental procedure

In this chapter the different experiments are described, explaining the procedures and parameters used in each one and the main characteristics of the devices.

For analyzing the SLM parts the next steps were done:

- Density measurements
- Aging treatment (half of the parts)
- Tensile test
- Optical analysis of the microstructure
- Hardness test
- SEM(Scanning electron microscope)
- XRD (X-Ray diffraction techniques)

3.1. Density measurement.

Density measurements are performed in order to have information on the absolute density of the parts. Also, one can obtain the relative density (%) of the parts, through a comparison between the theoretical density value of the alloy and the measured value. Relative density delivers information on the porosity of the samples. For AlSi10Mg alloys, the theoretical density value is 2, 68 g/cm^3

For measuring the density, Archimedes ´s method was used. The samples are measured in ethanol and in air. Previously, the density of ethanol must be checked, because the variations of the temperature or composition can give different values.

Then, with a simple formula, (1) one can calculate the absolute density of each part.

$$\rho_{abs} = \frac{m_{air} \cdot (\rho_{ethanol} - 0.0012)}{0.999836 \cdot (m_{air} - m_{summerged})} + 0.0012 \quad (1)$$

Where:

m_{air}= weight of the parts in the air(g)

$m_{submerged}$= weight of the parts in ethanol (g)

0.0012 g/cm^3= Archimedes density of the air.

For obtaining the relative density of each part, the following formula is used. (2)

$$\rho_{rel}(\%) = \frac{\rho_{abs}}{\rho_{theoretical}} \cdot 100 \qquad (2)$$

It is important to notice that sometimes bubbles of air entrapped inside the parts or at the surfaces can lead to a variation in the measurement, so it is necessary to wait until the displayed weight value is stabilized.

3.2. Aging treatment

Approximately half of the parts of each batch were aged. An aging of one hour at 175°C was done, and then the samples were cooled down in the furnace door closed until 70°C. After that they were air cooled.

The resistance air furnace 323 was used. For the measurements, shielded thermocouples plus an extra type K thermocouple were used, as well as a data logger in order to display and record the temperature into the furnace.

All parts were aged using the same program settings and furnace conditions. An aging of one hour above 170°C was done for half of the parts and then the samples were cooled down with the furnace door closed until 70°C. Firstly, the oven was preheated, and then the temperature was raised until 170°C for one hour. After that the parts were air cooled. Figure 5 shows the real temperature-time evolution.

The samples were placed inside the chamber with equal separation between them and in the horizontal edge position, to allow the most uniform heat distribution possible.

The aging allows diffusing atoms, that after they precipitate out of solution, as a reinforcing phase. So an increase in hardness should be expected due to precipitation of intermetalics in the matrix. The elongation and the other properties should not be compromised too much [BOH11].

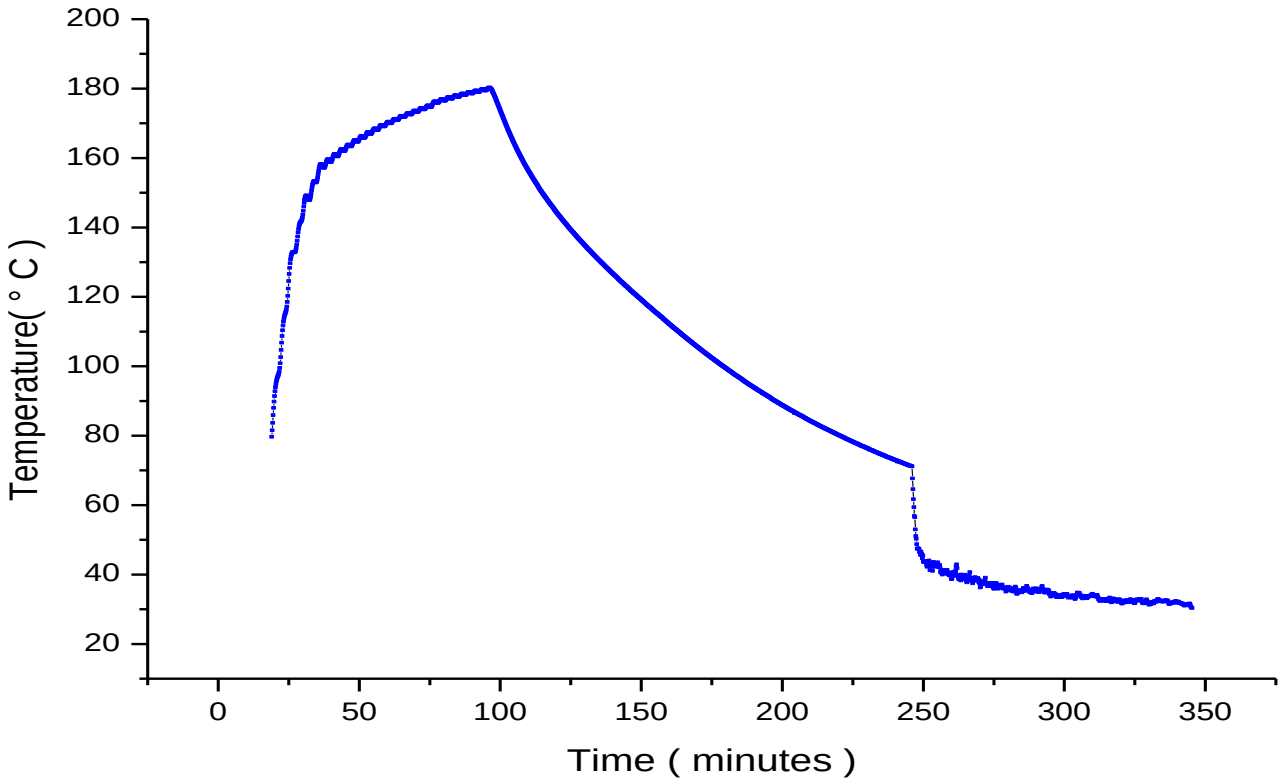

Figure 5 Temperature variation for the aging of AlSi10Mg parts.(1 hour, 175°C)

3.3. Tensile test

Tensile tests were performed on INSTRON 4505 machine. The deformation rate used was 1 mm/min, and an extensometer gauge length of 12, 5 mm was used in order to have an accurate measurement of the deformation of the sample.

By tensile testing, one can obtain information about E modulus, YTS (yield tensile strength), UTS (Ultimate tensile strength) and elongation to fracture. The stress-strain curve for an AlSi10Mg part made by SLM can be seen in Figure 6.

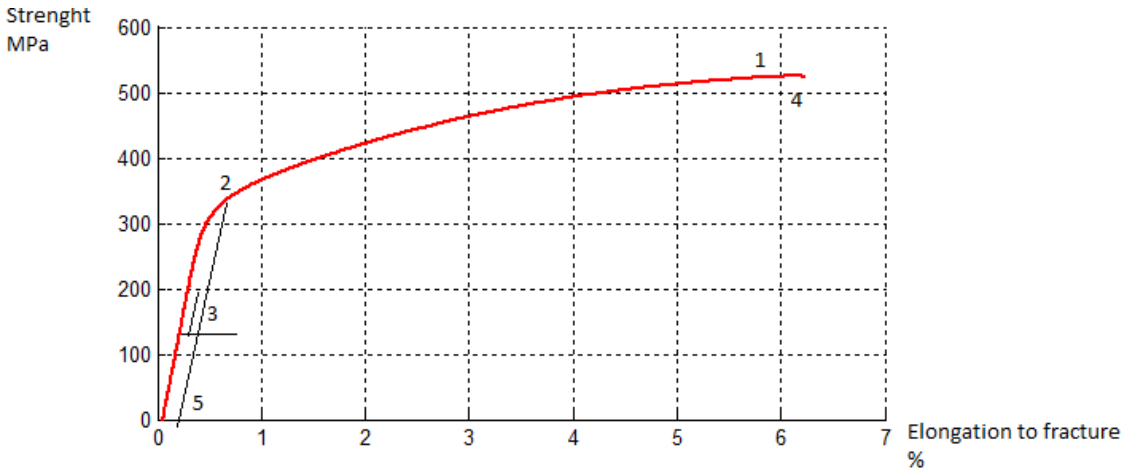

Figure 6 Stress-strain curve of a AlSi10Mg part made by SLM

The points in the figure correspond to the following:

1. Ultimate tensile strength (UTS): It is the maximum stress than the material can withstand in a tensile test.
2. Yield strength (YTS): It is the point at which the material starts to deform plastically.
3. Young modulus: It is the measure of the stiffness in the elastic region of the material. Correspond to the slope of the curve in the elastic region
4. Fracture: The point represents the maximum elongation to fracture.(x-axis)
5. Offstress strain (typically 0.2%)

3.4. Hardness test measurement

The goal was to measure the hardness of the parts, both in the building direction and scanning direction. This test gives a measurement of the resistance against deformation. The measures were taken according to the hardness Vickers scale.

Moreover, a comparison between the aged and no-aged parts, the traditional ones and between the different scanning modes and parameters can be established.

The equipment used for testing was FV700B. The parameters used are the following:

- Test Mode: VICKERS
- Test time: 10s
- Objective: X50
- Test Force: 0, 3 kg

3.5. Microstructure light optical analysis

For microstructure light optical analysis, the samples were observed with a polarizing microscope Axioskop 40 Pol/40 A Pol. The optical Lenses used are Carl Zeis X4, X10, X50, X100.

Figure 7 Optical microscope Axioskop[KUL13]

3.5.1. Preparation of the samples

For the preparation of the samples, first it was necessary to cut them. Two cuts of $1cm^2$ and a thickness of around 4mm were made on each sample, in order to obtain a top view in the scanning direction and a cross section oriented view in the building direction. A polymer was used to embed the pieces. For the part that was scanned on SEM, phenolic hot mounting resin with carbon filler was used. Using this thermoset

polymer with carbon, the sample becomes conductive as SEM analysis need. After that, parts were grinded and polished.

Figure 8 Crimping, (a) grinding (b) and polishing devices (c).

3.5.1.1. Etchants

The etchants used for the parts were HF, Keller's reagent and Barker´s reagent.

Keller's reagent is used for aluminum and aluminum alloys. It works good revealing the grain boundaries. It is based on a mixture of HF, HCl and HNO_3 with water. (Mixed as 1.0 mL HF and 1.5 mL HCl in 2.5 mL HNO_3 and 95 mL water). Barker ´s reagent was effective for visualizing the microstructure using polarized light in the optical microscopy. It is based on fluoboric acid with water.

The time of exposure to the etching agents was important in order to avoid overetching in the parts.

3.6. SEM (Scanning Electron Microscope)

SEM produces images of the sample using a focused beam of electrons, by the interaction of them with the sample. The microscope used was a PHILIPS scanning electron microscope XL30 FEG.

One piece (XY 0°NHT, no remelting) was scanned using SEM. With SEM, high resolution can be achieved, so detailed images as the grains in the heat affected zone or high magnification images of the pores could be obtained.

The surface of the part must be conductive to electrons. For this purpose, the polymer used to crimp the sample contained carbon, so the sample becomes conductive. A

pressure machine was applied in order to cure the polymer. In that way, some small kind of heat treatment could be done, because when one crimps using this machine heat is produced. But, taking into account the short time exposure, and the low temperature, one can neglect this “non desired” heat treatment.

3.7. X-ray diffraction techniques. Texture

By texture, one can determine and study the orientation of the grains of a piece. It can be represented using a pole figure. For measuring four samples (XY0°HT,XY0°NHT, Z90°NHT and Z0°NHT) the D500 goniometer was used, using a Cu tube at 40kV and 40mA. Pole figures were obtained for (111), (200), (220) and (311).

First, the samples were polished, and then the sample was taken out. Then the pieces were introduced inside a holder. For each sample the diffraction peaks were checked first. The results were analyzed in order to obtain the visual representation of the texture (pole figure).

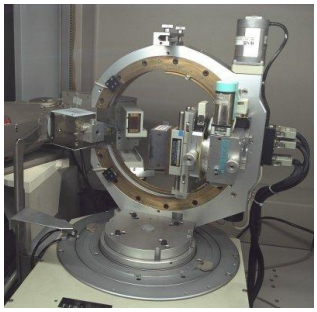

Figure 9 D500 goniometer was used in order to measure the texture of the AlSi10Mg samples. [KUL13]

4. Results and discussion

First a description of the batches that were tested is given. Next, a discussion of the influence of the scanning parameters and the scanning strategies in the mechanical and micro structural properties is done, using the results of the tests performed. Then the effect of the aging in hardness is specifically analyzed. However, the influence of the aging on other mechanical properties and on the microstructure of the parts is always discussed. The repeatability of the batches is also analyzed (when possible). Furthermore, the defects of the parts are analyzed, and a micro structural analysis by SEM is shown.

The obtained results of the SLM batches are always compared with the traditional casted parts.

4.1 Description of the batches

The batches that were analyzed, together with the main characteristics can be resumed in Table 5. Half of them were aged. In the table, one can see the different values for the power at which the pieces were built (200W, 240W, 290W and 300W), the scanning strategies, the building orientation and the scan speed. The scan speed is constant for A and B batches (1400mm/s). The scanning strategies figures and the building orientation figures can be seen in Figure 3 and Figure 4. Finally, the number of parts of each batch is shown. The scan spacing for all the batches was 105 um.

Table 5 Description of the different batches of AlSi10Mg parts by SLM that were analyzed. The machine used, scanning strategy, building orientation, power, scan speed and number of parts of each batch are given.

Batch	Machine used	Scanning strategy	Building orientation	Power (W)	Scan speed (mm/s)	Number of parts
A1	Concept Laser	Bidirectional long vector+remelting 90° rotated	XY	200	1400	6
A2	Concept Laser	Bidirectional long vector+remelting 90° rotated	Z	200	1400	6
A3	Concept Laser	Bidirectional long vector+remelting 90° rotated	XY	200	1400	5
A4	Concept Laser	Bidirectional long vector+remelting 90° rotated	XY	200	1400	5
A5	Concept Laser	Bidirectional long vector+remelting 90° rotated	Z	200	1400	6
B1	LMQ	Bidirectional long vector 60°rotated	XY	240	1000	1
B2	LMQ	Bidirectional long vector 90°rotated	XY	290	900	1
C1	LMQ	Bidirectional long vector 0°rotation	XY	300	1400	6
C2	LMQ	Bidirectional long vector 0° rotated	Z	300	1400	6
C3	LMQ	Bidirectional long vector 0° rotated	XZ	300	1400	8
C4	LMQ	Bidirectional long vector 60°rotated	Z	300	1400	6
C5	LMQ	Bidirectional long vector 90°rotated	Z	300	1400	6

4.2. Influence of the laser power

Previous studies establish a relation between the laser power and the porosity. Knowing the relative density one can have information about the porosity of each part, by comparing the absolute density value of each part with the theoretical density. For AlSi10Mg, the theoretical density is 2, 68 g/ cm^3.

The data corresponding to the relative density measurements of all the parts done by Archimedes can be seen in Table 6. They correspond to the batches that were produced with 200W (A3, A4, A5) while in Table 7 one can see the batches that were produced at 300 W (C series) in the LMQ machine. Furthermore, the graphical results are shown in Figure 10, where a comparison between the different batches can be seen.

Table 6 Relative density of A batches of AlSi10Mg parts. Average results with a confidence interval of 95% are shown

Sample	A3 (%)	A4(%)	A5 (%)
1	98,22	98,73	99,22
2	98,53	98,32	99,26
3	99,58	99,47	99,37
4			99,49
5			99,52
Average	**98,78**	**98,84**	**99,38**
Confidence interval	**0,41**	**0,34**	**0,06**

Table 7. Relative density (%) of C batches of AlSi10Mg parts. Average results have a confidence interval of 95%

Sample	C1 (%)	C2(%)	C3(%)	C4(%)	C5(%)
1	98,06	97,26	97,87	95,98	95,73
2	97,66	97,48	98,22	95,66	95,42
3	98,04	97,62	98,31	95,86	95,55
4	97,71	97,06	98,27	96,13	95,11
5	97,62	97,07	98,52	95,28	95,77
				95,97	95,38
Average	**97,82**	**97,30**	**98,02**	**95,08**	**95,05**
Confidence Interval	**0,10**	**0,11**	**0,11**	**0,12**	**0,10**

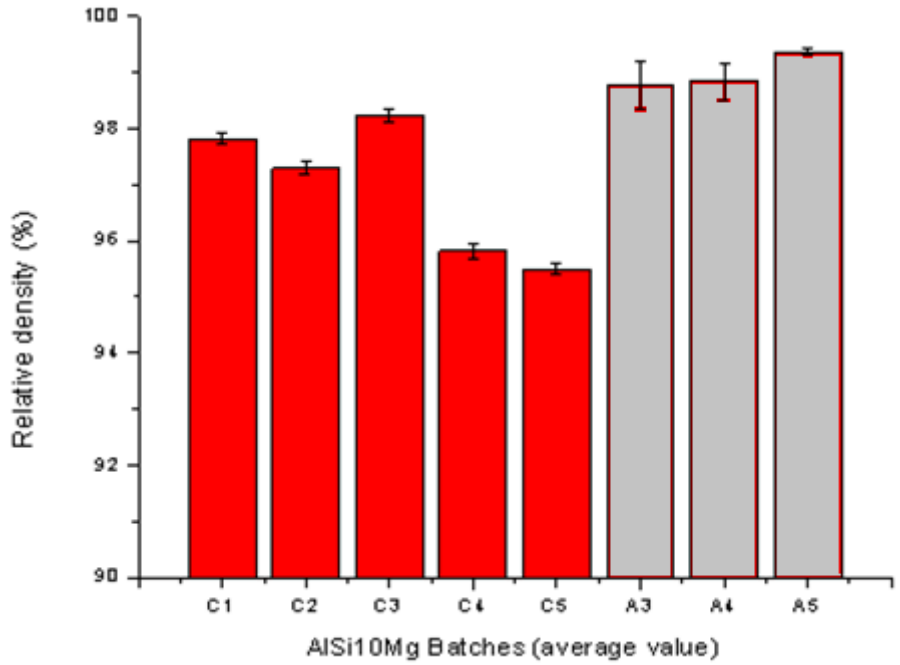

Figure 10 Comparison of the relative density (%) between different AlSi10Mg batches of parts produced by SLM

For A batches and C batches, the scan speed used was the same (1400mm/s). One can see that relative density is higher for the samples that were built at 200W rather than 300W. The results here show that for the same scan speed, higher relative density has

been reached with lower laser power. For C batches, the C4 and C5 batch (Z building direction, 60° and 90° rotation respectively) show the lowest relative density of the C batch. This could be due to evaporation processes and keyhole instability. When the laser power is increased, and considering that the rest of the scanning parameters are constant, the evaporation can increase, so more porosity will appear in the parts. Also, the keyholes are very unstable to the heat flow variations, so they could collapse easily at higher power causing keyhole porosity.

4.3. Influence of building orientation.

Here an analysis of the A,B and C batches is done, taking into account the mechanical properties obtained due to the tensile test that were done and the texture measured using X-ray diffraction techniques.

4.3.1. Influence of building orientation between A batches.

In Figure 4, the building orientations of the batch are explained. For A batches, XY and Z building orientations will be analyzed.

Looking at tensile test results one can see differences between Z and XY building batches. In Table 8 one can see the results for E, yield strength, UTS and elongation to fracture of the different A batches.

Table 8 Mechanical properties of the A batches of AlSi10Mg parts. Half of the parts were previously aged.

Batch	Building orientation	Thermal treatment	E(GPa)	Yield (MPa)	Elongation to failure (%)	UTS(MPa)
A2,A5	Z	Aged 170°C 1h	67 ±3	239 ±22	3,33 ±0,36	399 ±7

A2,A5	Z	-	67 ±5	227 ±26	3,69 ±0,26	406 ±5
A1,A3,A4	XY	Aged 170°C 1h	71 ±7	308 ±20	4,37 ±1,46	440 ±49
A1,A3,A4	XY	-	65 ±4	267 ±25	5,05 ±0,54	407 ±22

One can see that the elongation to failure of the Z oriented samples is in general lower than the XY oriented samples. While most of the XY samples are above 4%, the Z samples elongation to failure is below 4%. However, the confidence interval of the elongation to fracture of the XY aged oriented parts is ± 1,46%, due to a difference in the elongation to fracture results between (A3, A4) and A1 batches. Such a big confidence interval, for parts that were produced with the same parameters show that some kind of defect occurred for those parts, so the XY aged results will not be considered significant due to the dispersion presented. Thus, skipping the value of the XY aged parts one can say that the elongation to fracture for the XY parts is higher than the Z parts. It is expected that borderlines of pores will appear with more intensity at the start and end of the tracks, being more numerous for the Z oriented parts. Due to the faster strengthening in Z direction the fracture will be reached sooner for Z building oriented parts [KEM12].

UTS values of the samples analyzed here are higher than the highest values obtained by high pressure die casting with thermal treatment. While the range for casting is between 330 to 365 MPa, the samples by SLM that are being studied in this document are around 400 MPa and above. The elongation to failure of SLM remelted samples studied here is inside the range of the high pressure die casting and aged. The values of the casting parts to compare can be seen in Table

Related to the aging treatment, one can see that the yield stress is not significantly higher for the HT samples than for the NHT samples for this aging treatment. The yield

stress of the aged batches it is 273, 5 ± 34,5 MPa, while for the non aged parts is 247 ± 20 MPa. However the differences are not significant.

One can conclude for the A batch, that Z building oriented parts shows lower elongation to failure than XY oriented parts. In Z building parts, more borderline porosity at the beginning and ending of the scan tracks could be the main cause of the fracture. Less elongation to fracture for Z oriented part will be reached. Higher level of stress in Z oriented part (due to faster strengthening in Z direction) will be reached sooner in the borderline of pores. Those pores will be the origin of the complete fracture of the part when doing the tensile test. The porosity will be studied with more detail in the next pages.

4.3.2. Influence of building orientation between C batches

The influence of the different building orientations (XY,Z,XZ) of the C batches can be analyzed taking into account the results of the tensile test that were done. In Table 9 the E modulus, yield strength, elongation to failure and UTS of the different batches can be seen.

Table 9 Mechanical properties of the C batches parts of AlSi10Mg produced by SLM.

Batch	Building orientation	Thermal treatment	E(GPa)	Yield (MPa)	Elongation to failure (%)	UTS(MPa)
C2	Z	-	71±1,31	209±5,64	3,34±0,25	386±6,69
C2	Z	Aged 170°C 1h	73±4	178±32	4,78±0,68	407±2,5

C1	XY	Aged 170°C 1h	69 ±0,37	264 ±10	4,71 ±1,4	436 ±18
C1	XY	-	68 ±3	254 ±15	5,08 ±1,6	457 ±11
C4	Z	Aged 170°C 1h	71 ±0,67	144 ±12	3,99 ±0,57	360 ±14
C4	Z	-	72 ±4	216 ±76	4,146 ±0,24	395 ±59
C5	Z	Aged 170°C 1h	69 ±2	153 ±1	4,11 ±0,13	350 ±6
C5	Z	-	68 ±0,37	167 ±11	4,28 ±0,19	348 ±11
C3	XZ	Aged 170°C 1h	72 ±0,45	295 ±14	5,80 ±1,10	445 ±22
C3	XZ	-	71 ±2	307 ±4	5,465 ±0,74	450 ±7

For the C5 batch, one of the parts shows a strange behavior during the tensile test. It seems that some problem happened during the tensile test or during the production of the part, so it is not taken into account. This strange behavior however can be seen in Figure 14. For having a graphical overview of the different C batches the results are shown in Figure 11, Figure 12, Figure 13, Figure 14, and Figure 15.

One can see in the figures that the results between the parts of the same batches are similar for C2 batch, C5 and C4 batches.

The elongation to fracture presents more variations between the parts of the same batches. This can be seen graphically and looking at the confidence intervals shown in Table 9. For C3 batch aged, the elongation to fracture is 5,80 ±1,10, which means a confidence interval of 19% over the obtained measure. Also, for C1 batch, the confidence intervals are high: 4, 71 ±1, 4(%) for the aged parts and 5,08 ±1,6(%) for those that were not aged.

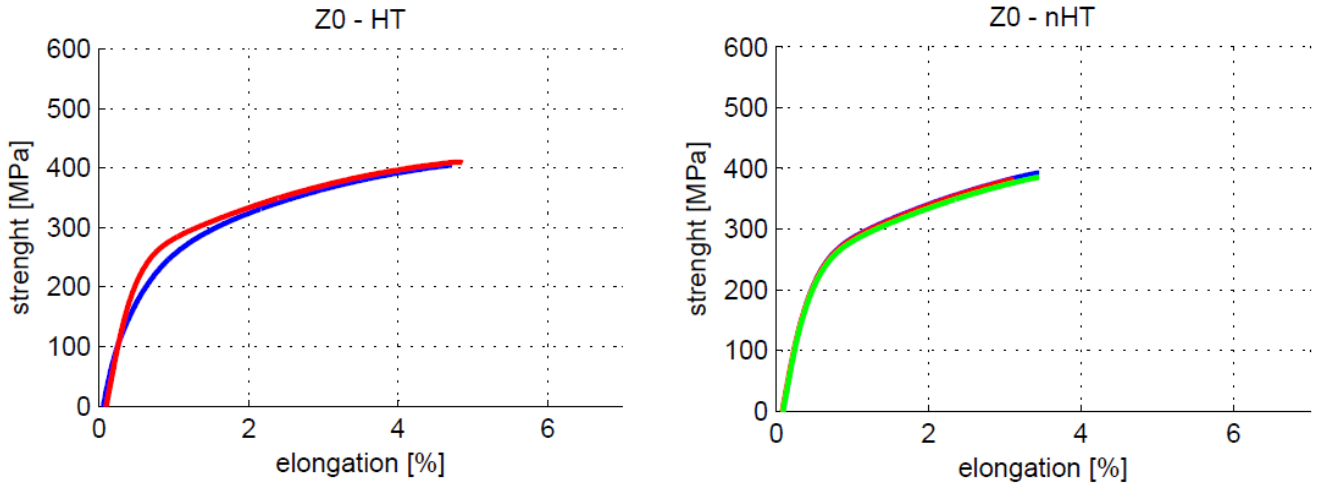

Figure 11. Stress-strain curve of C2 batch (Z oriented,0° rotation), AlSi10Mg. The samples of the left picture were previously aged (175°C, 1hour)

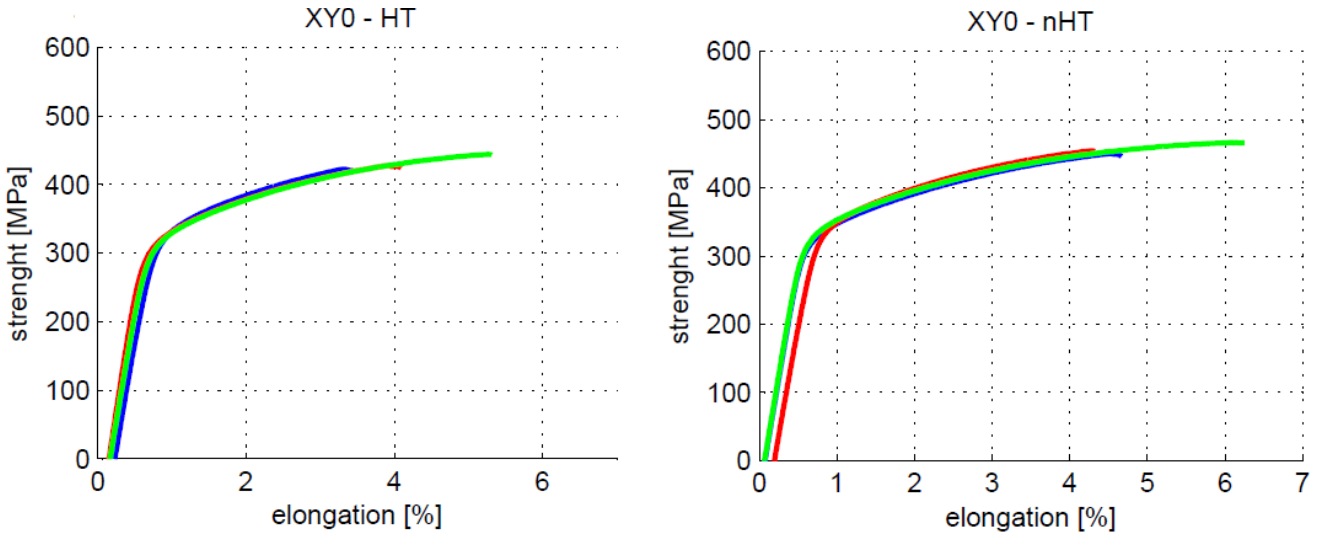

Figure 12. Stress-strain curve of C1 batch (XY oriented,0° rotation), AlSi10Mg. The samples of the left picture were previously aged (175°C, 1hour)

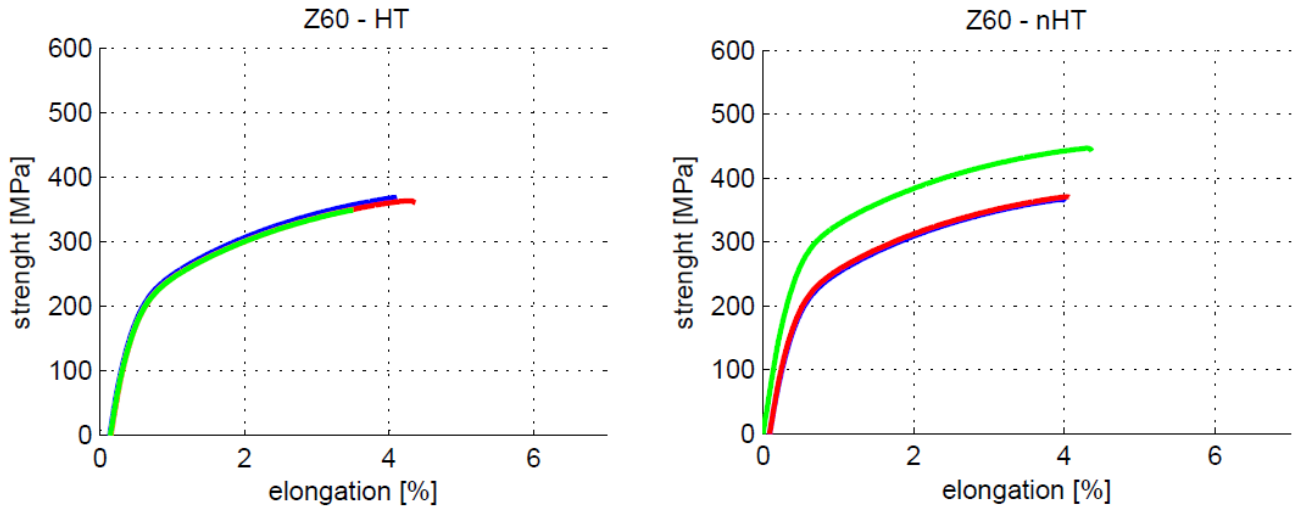

Figure 13. Stress-strain curve of C4 batch (Z oriented, 60° rotation), of AlSi10Mg parts The samples of the left picture were previously aged (175°C, 1hour)

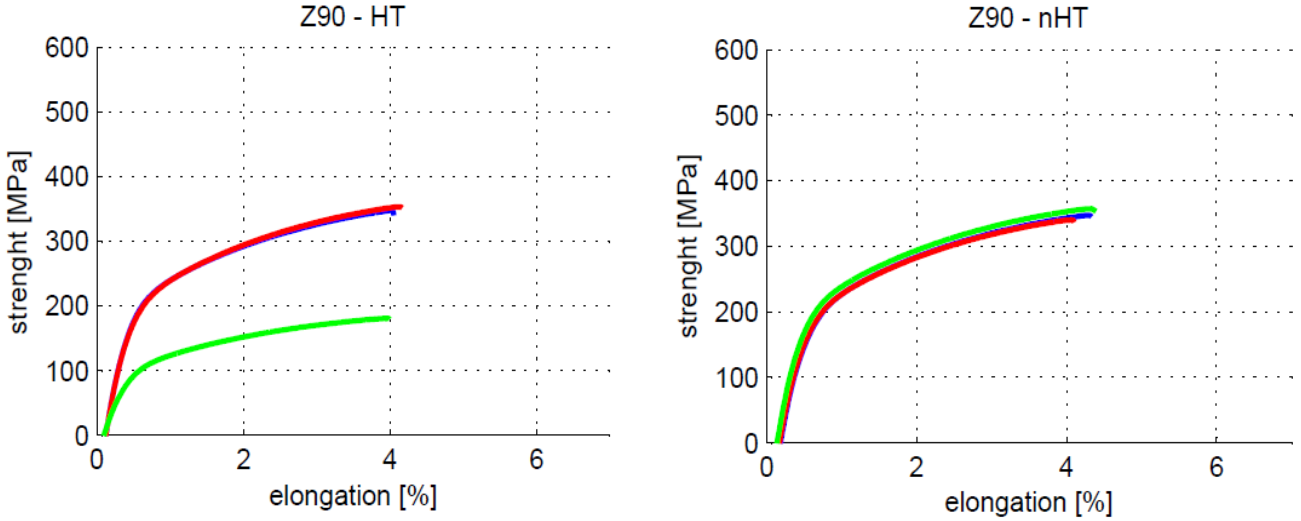

Figure 14. Stress-strain curve of C5 batch (Z oriented,90° rotation), of AlSi10Mg parts. The samples of the left picture were previously aged (175°C, 1hour)

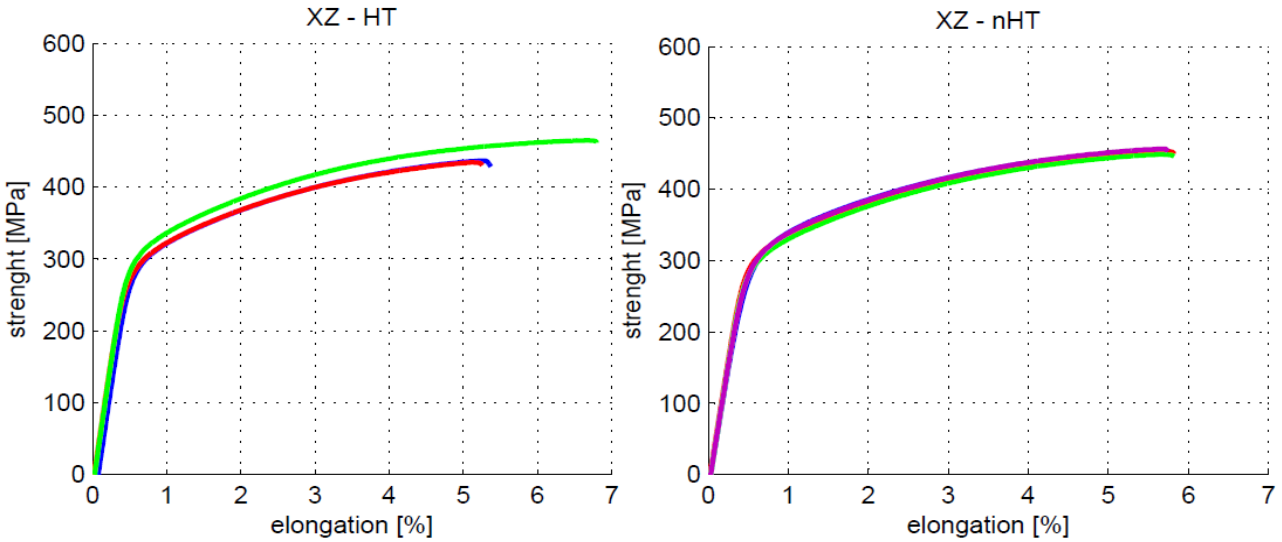

Figure 15. Stress-strain curve of C3 batch (XZ oriented,60° rotation), AlSi10Mg. The samples of the left picture were previously aged (175°C, 1hour)

Here a comparison between the different batches is done, separating heat treated and non heat treated parts. Also, die casting+ aged parts are included (considering the mean values of the possible ranges for casting):

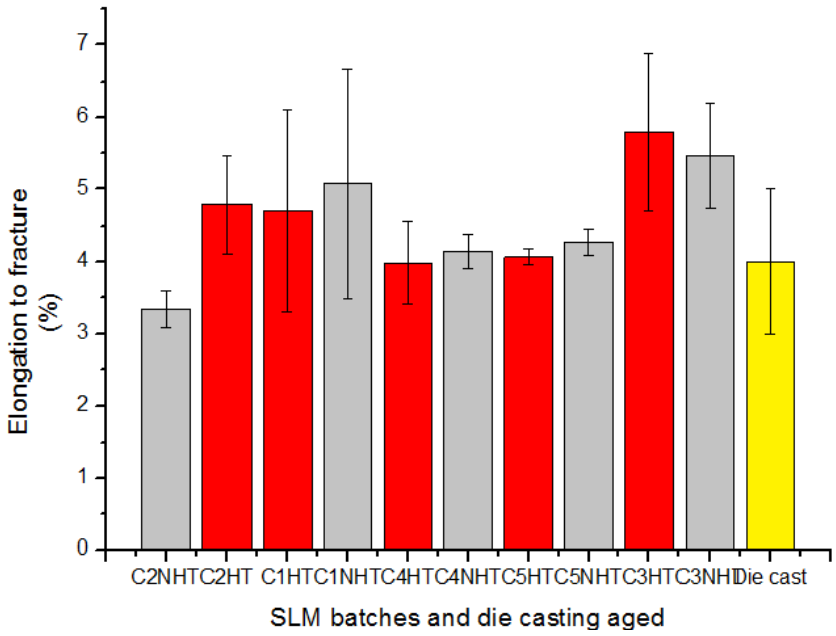

Figure 16 Elongation to fracture. Comparison between SLM batches and die casting+aged values. Only maximu m value of the die casting + aged range are taken into account. The range is (3,5-5 %) [KEM12]

One can see that the maximum elongations to fracture values are obtained for C3 batch (XZ oriented, rotation 60°), while the minimum values are obtained for the C2 non-aged parts (Z oriented, rotation 0°).

Z building direction parts have the lowest elongation to fracture values. This can happen, according to [KEM12], due to the presence of more borderline porosity in Z oriented parts. Due to the optimal density strategy chosen when building, more concentration of defects, forming borderlines of pores at the beginning and end of the tracks appear, and these pores will initiate later the fracture.

Looking at the results, only significant difference between the aged and non aged parts is found for the C2 batch. However, for the rest of the batches no significant differences between aged and no-aged parts are found.

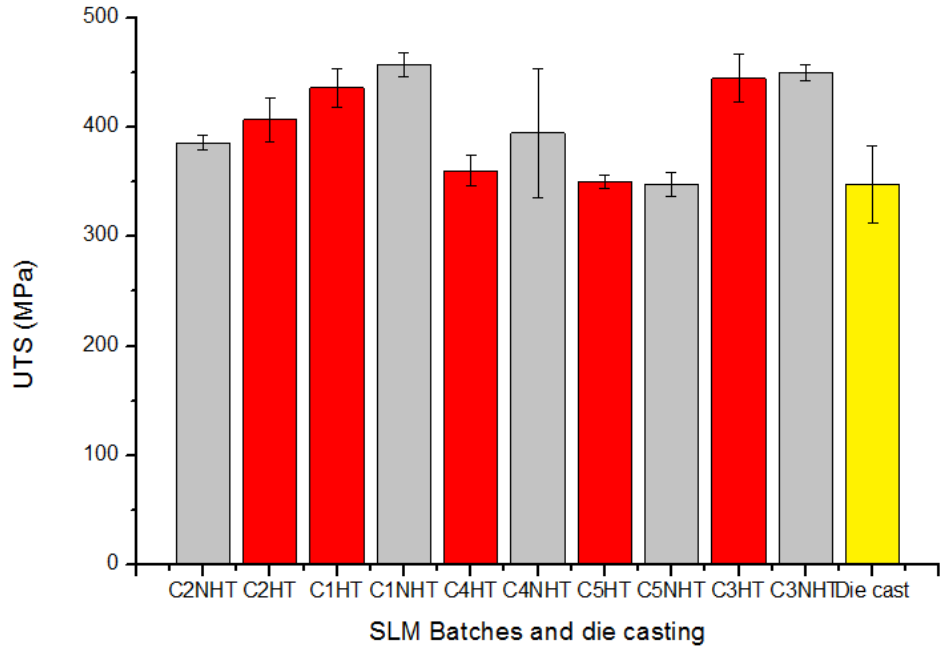

Figure 17 UTS comparison between SLM batches and die casting of AlSi10Mg. Average values of the range 330-365Mpa [KEM12] of die casting+aged parts are given.

For Ultimate tensile Strength, one can see moderate differences between the batches. The values of UTS are equal or higher than the die casting+ aged parts. The UTS range of die casting is 330-365[KEM12], so all the SLM parts studied here are above UTS values of die casting+aged parts.

Looking at the results one can conclude, as it was said before, that the XY and XZ parts show slightly higher elongation to fracture than the Z parts. However, taking into account the confidence interval one could say that is not a significant difference. No significant differences were found for the aged and non aged parts. Compared with the die casting+aged parts, the SLM C batches show equal or higher mechanical properties.

4.4. Influence of the aging in hardness.

The influence of the aging in the hardness of SLM parts will be analyzed here. Four samples from A4 (XY oriented) and A5 (Z oriented) batches were analyzed. Half of them were aged at 175°C during 1 hour, and then slowly cooled down. The details of the aging can be seen in Figure 5

The results can be seen in Table 10.

Table 10 Hardness of A4(XY oriented batch) and A5(Z oriented batch). AlSi10Mg parts produced by SLM. Four parts were analyzed, two aged and two no aged.

x ± s	HV	Confidence interval
A4 (XY direction) HT	157	3,54
A4 (XY direction) NHT	152	3,05
A5 (Z direction) HT	143	3,04
A5 (Z direction) NHT	135	2,78

In high pressure casting + aging parts, the AlSi10Mg alloys are hardened by the formation of Mg_2Si precipitates during an aging treatment. Those precipitates contribute to harden the matrix without compromising too much the rest of the mechanical properties. However, in SLM, the high hardness is reached due to the fine dispersion of the Si in the Al phase.

Taking into account the confidence interval, one can only say that the difference between aged and non aged SLM parts is very small. Also it is observed anisotropy in the XY and Z oriented samples. Higher values are obtained for the XY direction samples studied here. The reason could be due to the different microstructure due to the different scanning strategy between the Z oriented parts and the XY oriented parts. Variations in the heat flow between the XY oriented and Z oriented will affect the micro structure of the parts. These differences in heat flow can be possibly due to the different track length (Z oriented tracks are shorter) and could affect the microstructure, being the main reason of the difference in hardness.

The hardness test also shows that higher values are obtained for all the SLM parts studied here in comparison with the best traditional cast. ones (high pressure casting +

aging). This happen because SLM provides a very fine dentritic solidification microstructure due to the high thermal gradients while building the samples, which lead to very good properties. [KEM12]. The comparison data with traditional casting are shown in Table 11 and Figure 18

Table 11 Hardness of AlSi10Mg casting samples [KEM12]

x ± s	HV
conventional cast and aged	86
high pressure die casting	95-105
high pressure die casting and aged	130-133

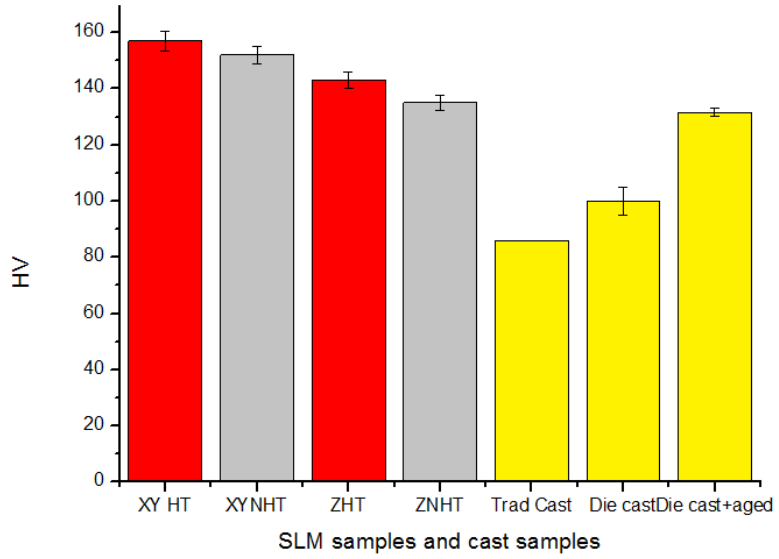

Figure 18 Comparison between SLM samples & cast samples. Average values of the range are taken into account for casting samples.

4.5. Reproducibility of the Batches.

For analyzing the reproducibility of the batches A1,A2, A3, A4 and A5 batches can be compared.

In Figure 19 ,Figure 20, Figure 21 and Figure 22 one can establish a graphical comparison between the different batches. While blue colored correspond to A1 and A2 batches, red colored correspond to A3, A4, and A5 batches which were analyzed two months after the A1 and A2 batches.

Although all A batches were done with the same scanning strategy, power and scan speed, one can see differences between them.

One can observe that there is a big difference in the elongation to fracture between A1 batch and (A3, A4) batches, for those which where aged, which can only be explained due to a problem when they were manufactured. Also, for those which were not aged, one can observe in Figure 20 a noticeable difference between the batches in UTS. One possible explanation is because they are from different batches manufactured in different periods of time, so the composition could vary a bit from one batch to another.

A complete comparison between A2 and A5 batches (the ones which were built in Z direction), is not possible because mostly A5 parts should be rejected due a defect while manufacturing, so only two parts are available (one aged, and other no aged). However, looking at the stress strain in Figure 21 and Figure 22 for those parts that could be tested one can see that the accuracy between the A5 and A2 batches is better.

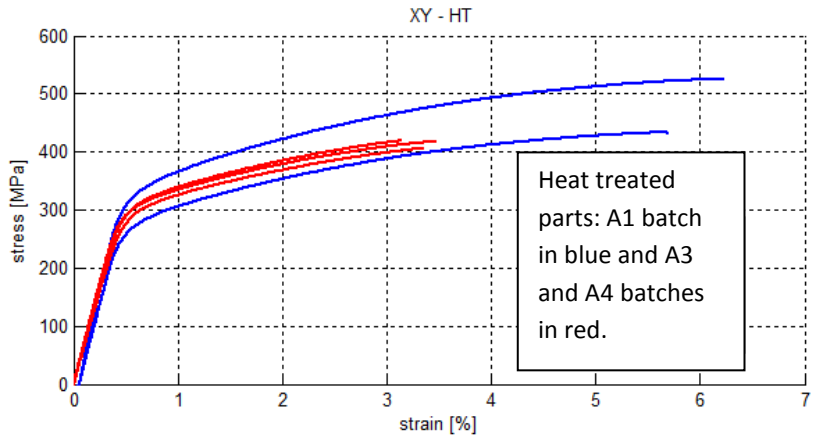

Figure 19 Stress-strain curve of A1, A3, A4 AlSi10Mg batches.(XY building orientation, remelted with 90°rotation) The parts were previously aged. (170°C, 1 hour).

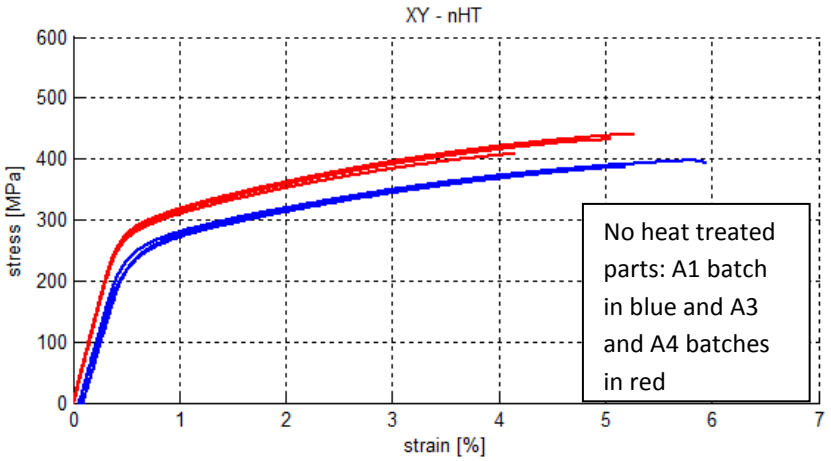

Figure 20 Stress-strain curve of A1, A3,A4 AlSi10Mg batches.(XY building orientation, remelted with 90°rotation) The parts were not previously aged.

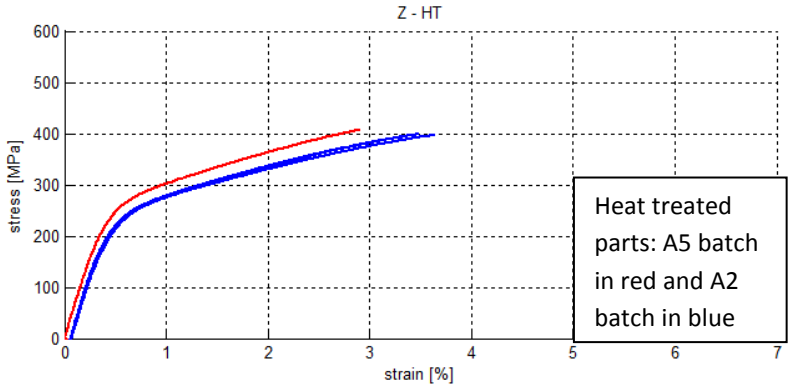

Figure 21 Stress-strain curve of A2, A5 AlSi10Mg batches (Z building orientation, remelted with 90°rotation) The parts were previously aged (1 hour, 170°C) .

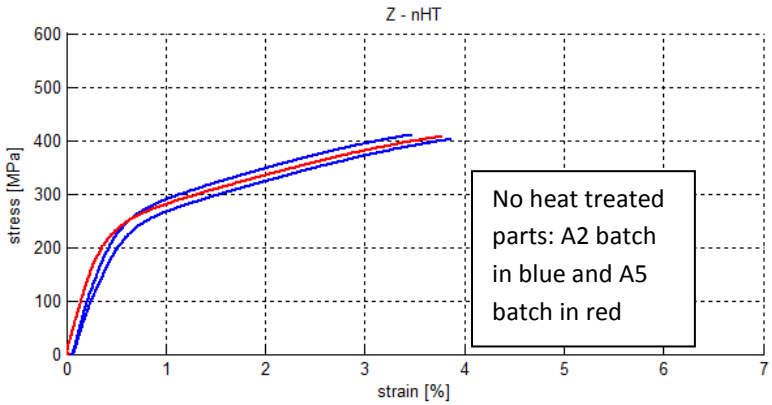

Figure 22 Stress-strain curve of A2 A5 batches of AlSi10Mg parts. The parts were not aged.

4.5.1. Issues noticeable during tensile test of A batches.

The samples of A5 batch (Z oriented) presented a defect in one of the sides, that was produced during the fabrication process. This defect could happen when the production is suddenly stopped while manufacturing the part and later on is continued. Due to this defect the most of pieces were broken when clamping in the machine and they were rejected

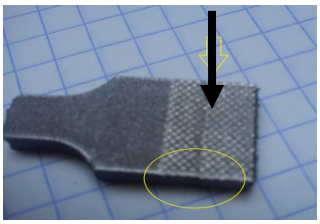

Figure 23 Issues in A5 batch (Z oriented 90rotation samples.) Due to defects in production most of the samples were broken when clamping.

4.6. Influence of the scanning strategy.

The different scanning strategy used should affect the microstructure of the different batches and the texture, showing the tracks and the grains orientations. Below, some images of microstructures are shown in order to analyze and discuss the different tracks structures.

4.6.1. A3 batch. Top view

In Figure 25the remelted structure is clearly shown, with the tracks perpendicular between them due to the rotation of 90°.At this magnification level, one cannot see differences in the microstructure due to the aging.

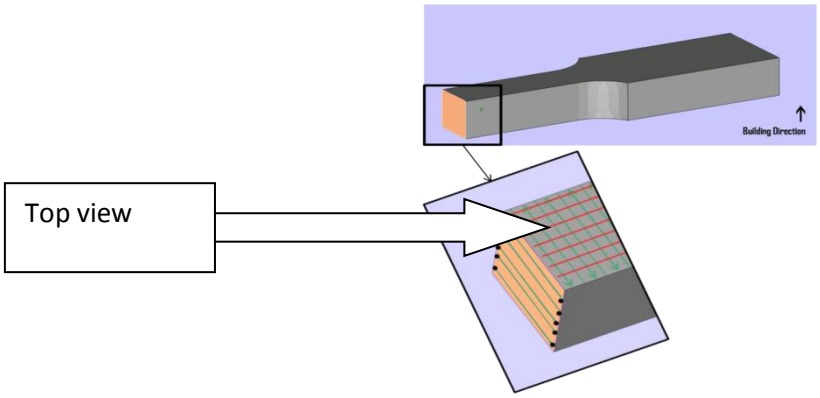

Figure 24 Schematic view of Top View of XY oriented parts[KEM12]

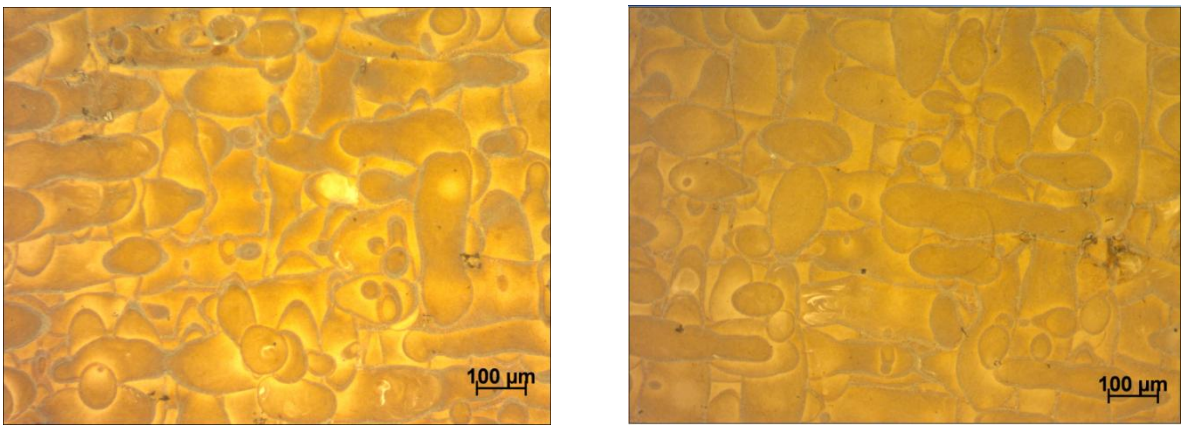

Figure 25. Microstructure of AlSi10Mg by SLM. Top view of the A3 batch. The left image was aged(170°C,1 hour).

4.6.2. A5 batch. Z cross Section

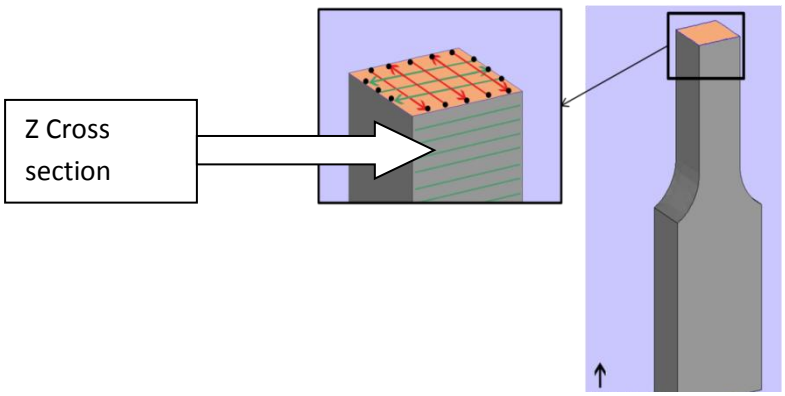

Figure 26Scchematic view of the Z cross section of the side view[KEM12]

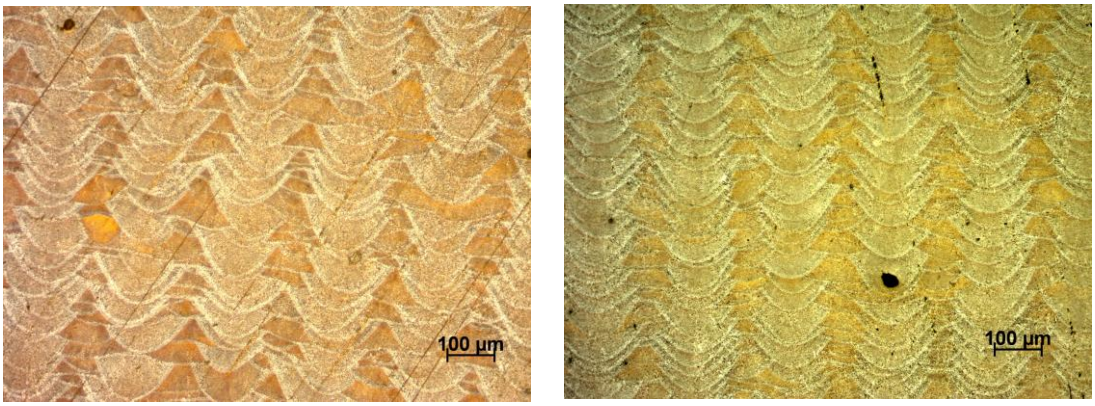

Figure 27 Microstructure of AlSi10Mg by SLM. Cross section view of A5 batch. The part of the left image was heat treated (aging, 170°C, 1 hour).

In the Z cross section of the side view (batch A5), one can observe in Figure 27 the half pipe form of the melt pool produced by the laser scan.

Again, at this magnification no differences between the aged and no aged parts are visible in Figure 27

4.6.3. B2 Top view and Cross section.

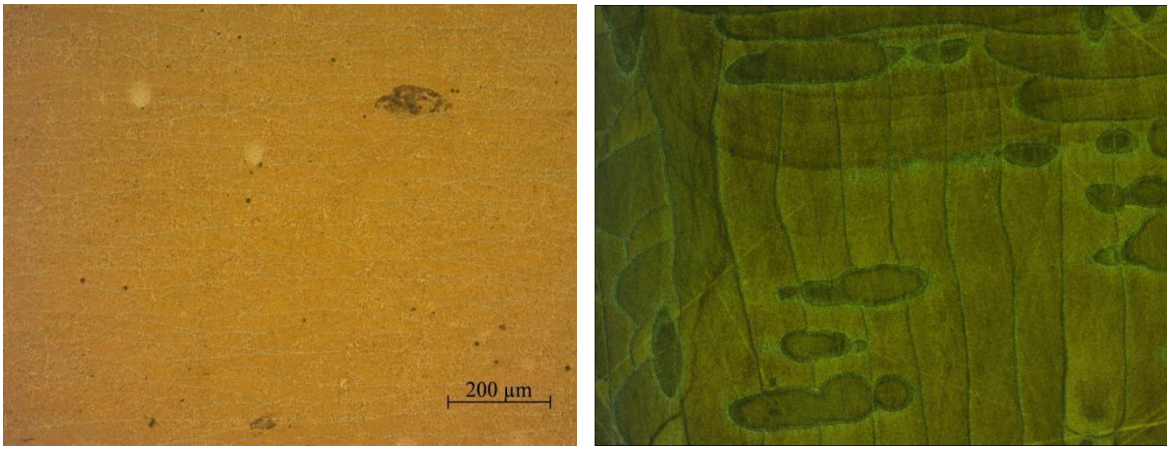

Figure 28 Microstructure of AlSi10Mg by SLM. View of B2 batch. The left image shows the cross section (HF etched) and the right image the top view (Barkers etching with polarized light)

In Figure 28 the scanning strategy is shown: rotation with no remelting between layers. The angle of rotation was 90°. The tracks are clearly visible in the right figure, while the half pipe form the melt pool can be seen in left image. The right figure was etched

which Baker s and a polarized light was used to reveal the laser tracks. White spots that are visible in the left image are due to a bad etching in these zones.

4.6.4. B1 Top view

Figure 29 Microstructure of AlSi10Mg by SLM. Top view of B2 batch.

The sample shown on Figure 29 was etched with Kellers, which revealed very effective to show the grain boundaries. The orientation of the grains is clearly shown in the picture, and also the rotation between layers, without remelting.

4.6.5. Texture

An analysis of texture has been done for C batches. Four parts were analyzed.

- One sample of batch C1 that was aged.
- One sample of batch C1 that was not aged
- One sample of batch C2. No aged
- One sample of batch C5. No aged

  While C1 and C2 parts are built without rotation between layers, C5 batch was rotated 90° between layers.

4.6.5.1. C1 Part. Aged (No rotation between layers, XY oriented.)

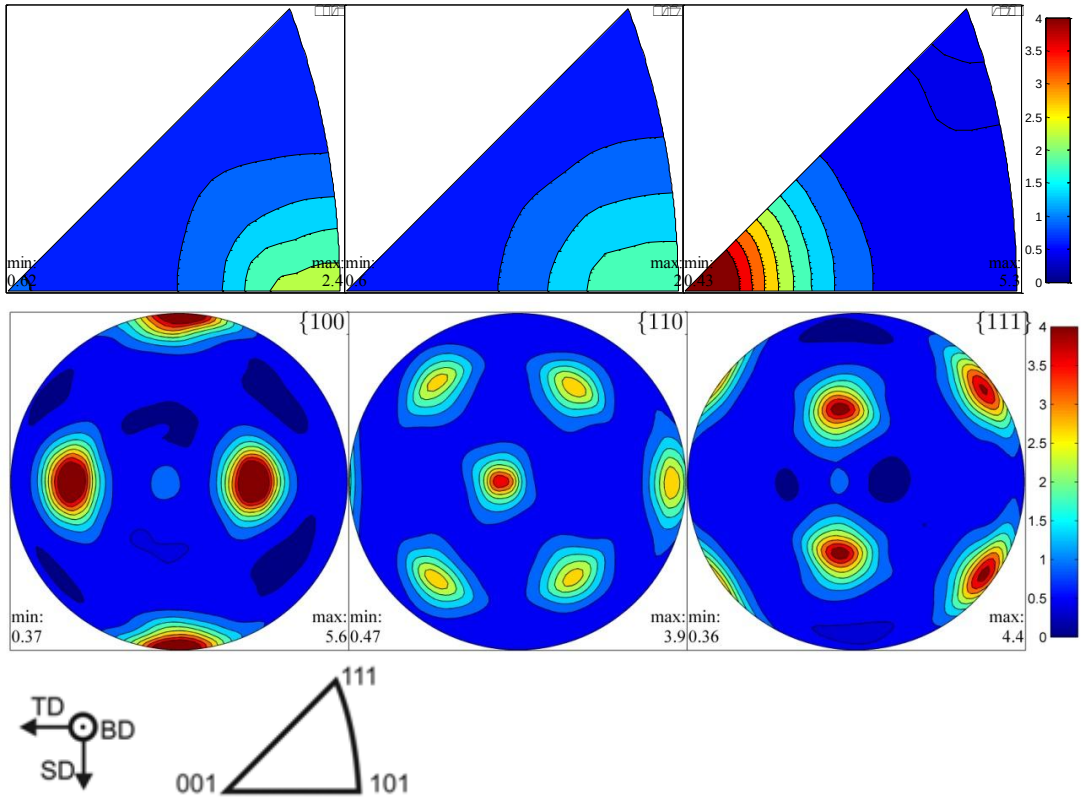

Figure 30 Pole figures(up) and inverse pole figures(down) for AlSi10Mg SLM part produced with no rotation between layers. The part was aged (175°C,1hour).

4.6.5.2. C1 Part Non-Aged. (No rotation between layers, XY oriented.)

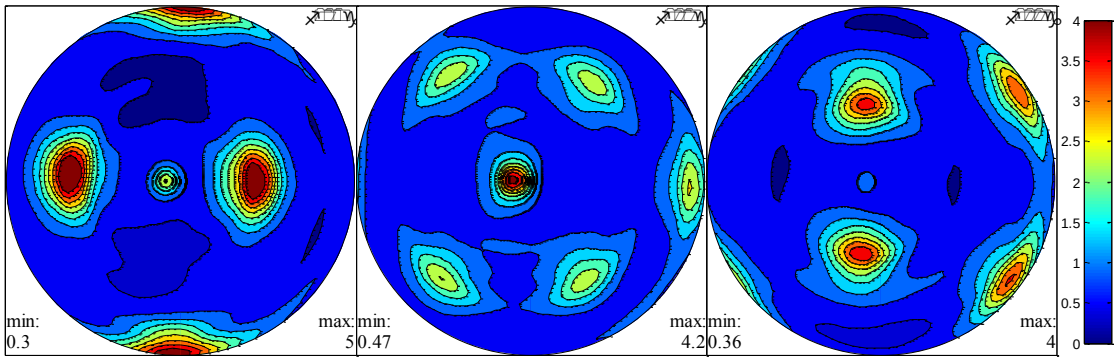

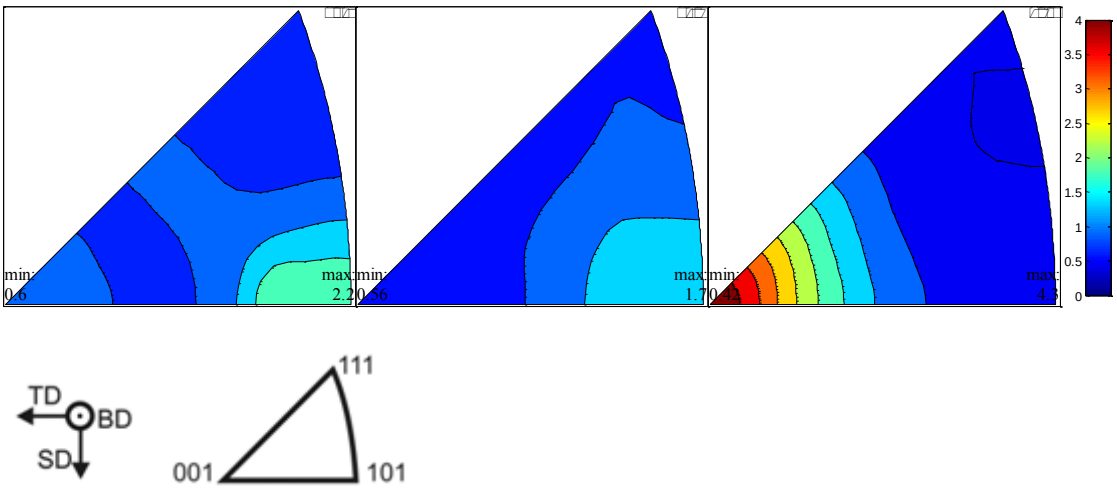

Figure 31 Pole figures(up) and inverse pole figures(down) for AlSi10Mg SLM part corresponding to batch C1 produced with no rotation between layers. The part was not aged.

4.6.5.3. C2 Part. (No rotation between layers, Z oriented.) No aged.

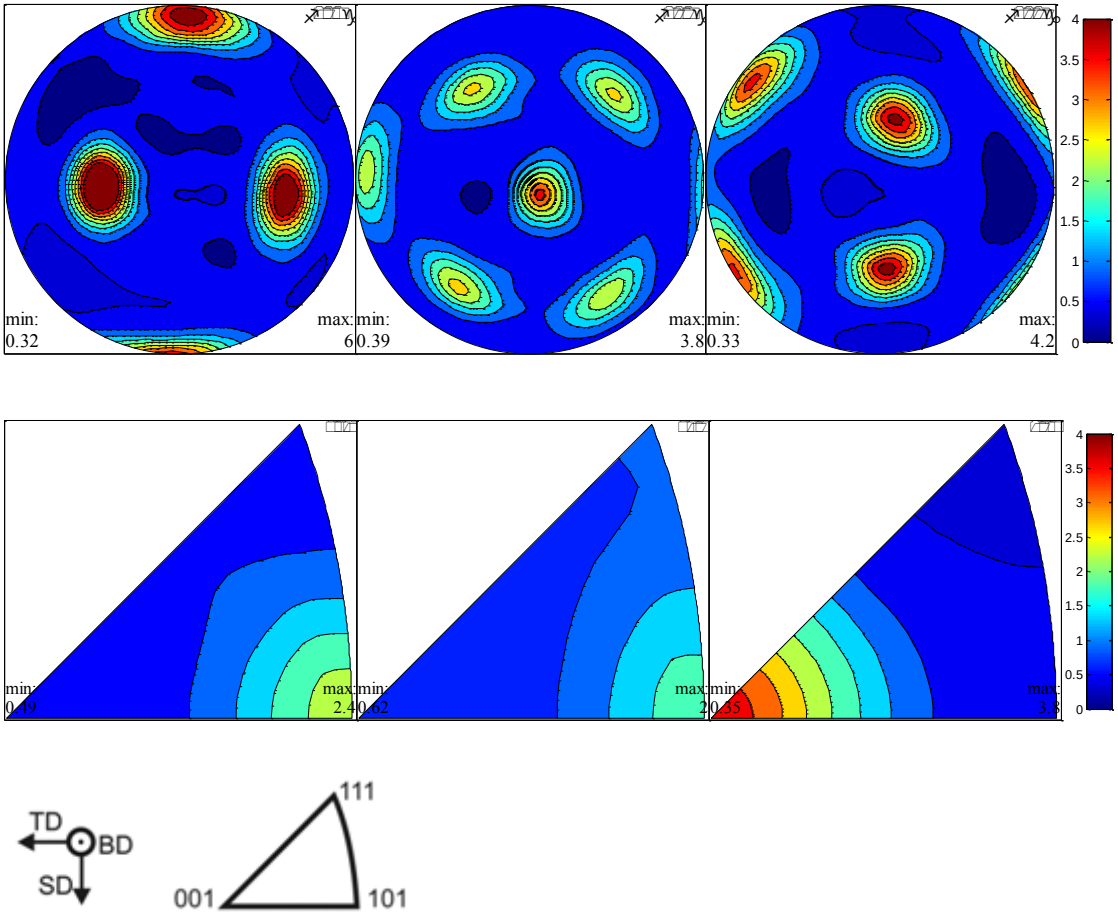

Figure 32 Pole figures(up) and inverse pole figures(down) for AlSi10Mg SLM part corresponding to batch C2 produced with no rotation between layers. The part was not aged

Taking into account the scanning direction, one can see that for the parts that were built without rotation between layers, there is a strong <100> texture in the scanning direction, that can be seen clearly in the inverse pole figure (100), parallel to the scanning direction. There is also a weaker texture <110> parallel to the building direction.

Related to the heat treatment that was done for the second C1 part it should not affect the texture in a significant way because the temperature was 175°C, below the recrystallization temperature. The results shown here shown that no significant differences in texture are obtained for the aged and non aged part.

4.6.5.4. C 5 Part. (Rotation between layers, Z oriented.)

Batch C5 parts were rotated 90° between layers when building. One can see that the texture orientation of the grains in the scanning and the building direction is not so clear as in the previous parts that were produced without rotation between layers.

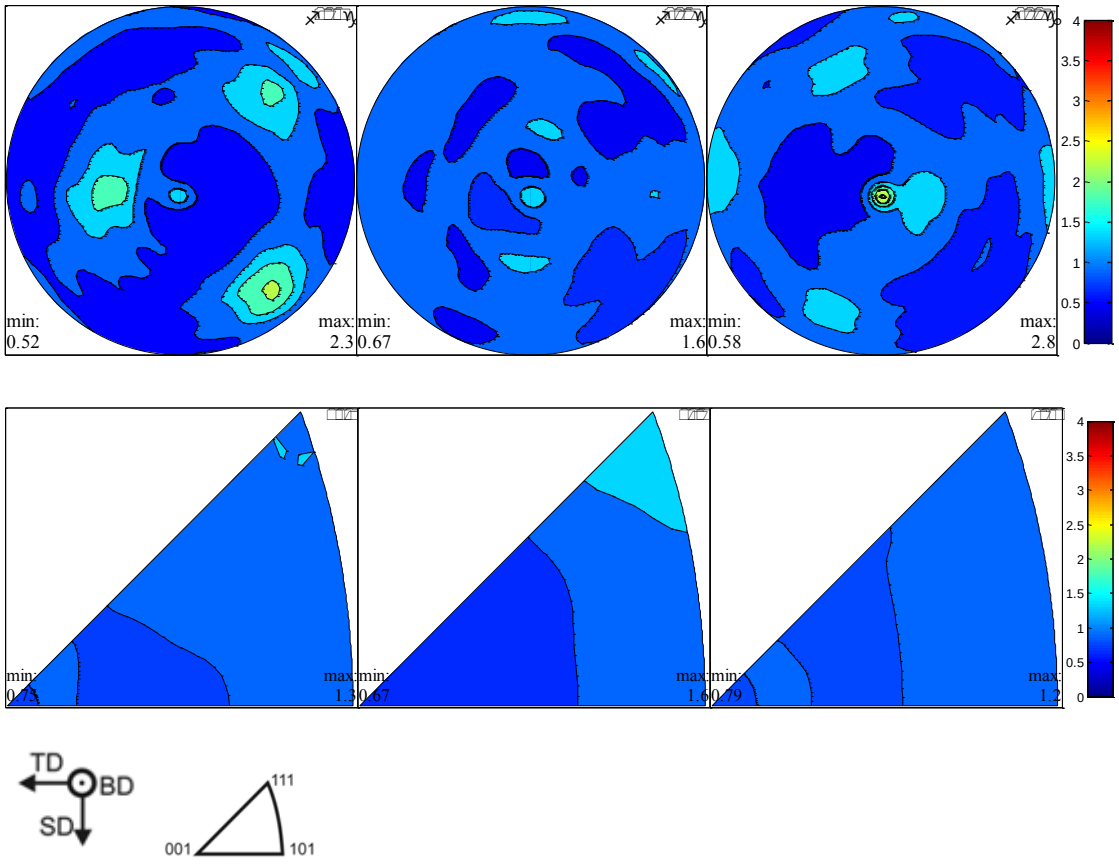

Figure 33 Pole figures(up) and inverse pole figures(down) for AlSi10Mg SLM part corresponding to batch C5 produced with rotation between layers. (90°). The part was not aged

4.7. Defects and SEM analysis

For analyzing defects the structure of the A and B batches was analyzed using the optical microscope. SEM was used in order to study the melt pool.

Figure 35 correspond to the top view of the A5 batch. The details of the plane that is being analyzed can be seen in Figure 34.

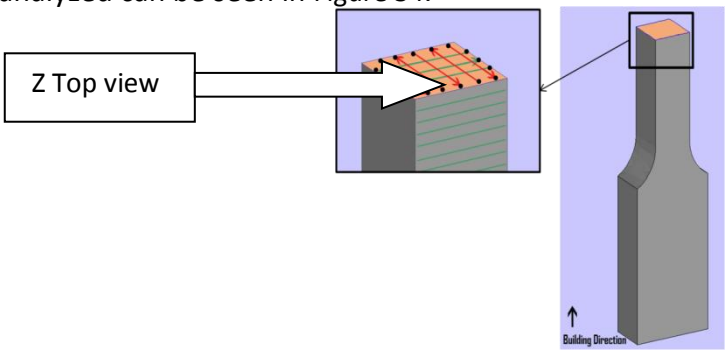

Figure 34 Schematic view of the Z Top view[KEM12]

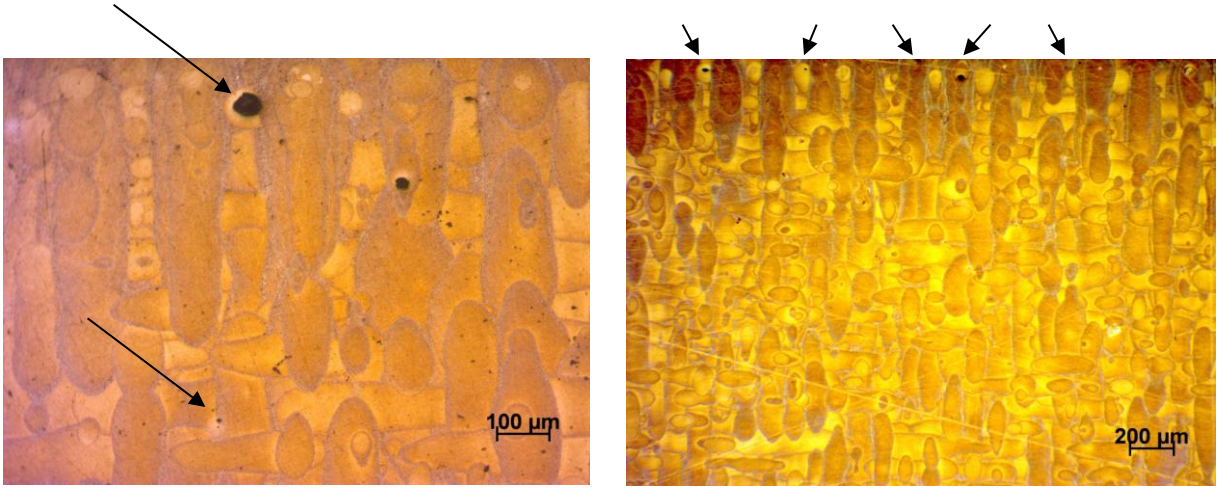

Figure 35 Microstructure of AlSi10Mg by SLM. A5 batch Top view. The image of the right was heat treated (aged, 170°C, 1 hour) A keyhole pore can be seen in the left image. At right, a borderline of pores is clearly shown.

In Figure 35 different types of porosity can be seen. One can see spherical pores as a consequence of entrapped gasses or evaporated powder during the melting process. They are located within the melt pools. [KEM11]. Keyholes pores also can be seen. They are formed due to imperfect collapse of keyholes. Key holes are very unstable, so a variation in the temperature equilibrium can lead to the creation of larger pores [THI12]. This will happen more frequently in the beginning and ending of the scan

tracks due to more heat flow variation in these zones, as one can see in Figure20. Turbulent flow has been linked with the porosity formation. [ZHA01]

In Figure 36 one can observe clearly the presence of more porosity at the beginning/ending of the melt pool tracks, forming borderlines of pores situated in these places.

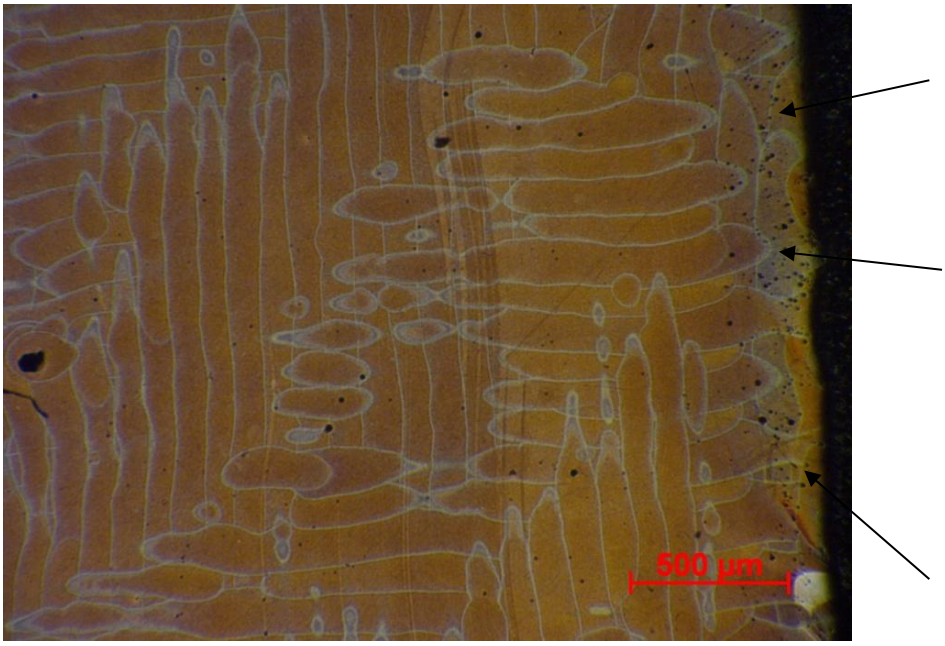

Figure 36 Microstructure of AlSi10Mg by SLM. Top view of the B1 batch. One can see the presence of more pores at the beginning of the tracks, forming a borderline of pores. This could be due to heat flow variations and evaporation phenomena.

A keyhole pore from B2 batch can be seen with higher magnification in Figure 37 . As it was said before, the instability of the keyholes leads to the collapse of keyholes and to the formation of keyhole pores due to heat flow turbulences. Keyhole instability is also related with the surface tension pressure, which contributes to close the keyhole and the vapor pressure, which tends to maintain it open. The aluminum alloys have a relative high surface tension and low vapor pressure so the keyholes are relatively easy to collapse. [ZHI01]

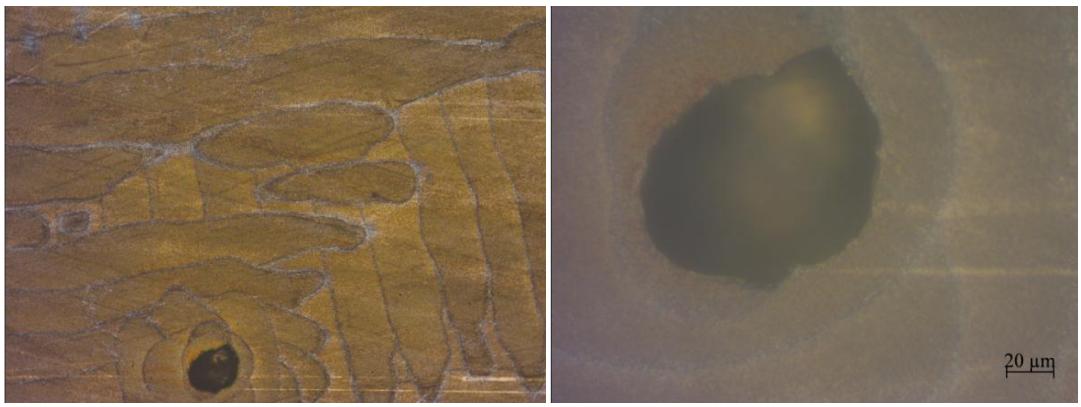

Figure 37. Microstructure of AlSi10Mg by SLM. B2 batch Top view. Detail of a keyhole pore(right image)

Oxides are produced due to the presence of small amounts of oxygen when the parts are produced. In these two images, a big defect can be shown. Also some oxides can be seen. More oxides are shown for the Top view of A3 batch (XY orientation). More oxides can be seen in Figure 39

Figure 38 Microstructure of AlSi10Mg by SLM. B1 batch. Cross section view(left) & top view(right). In the left images some oxides can be seen. In the right a big defect can be seen.

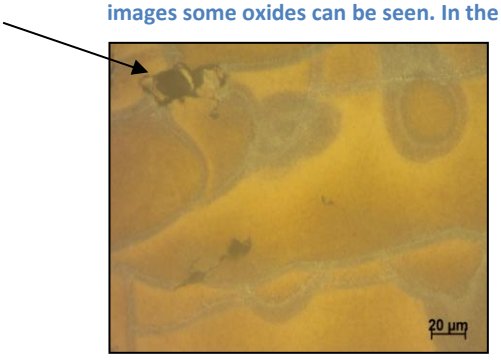

Figure 39. Microstructure of AlSi10Mg by SLM. Top view of A3 batch. The arrow shows an oxide, due to the presence of small amounts of oxygen.

In Figure 41 one can see both spherical pores and irregular pores. Irregular pores are created by unmelted powder and by insuficient overlapping between the scan tracks[KEM11]. Also, one can see oxides due to the presence of small percentages of oxigen during the production process.

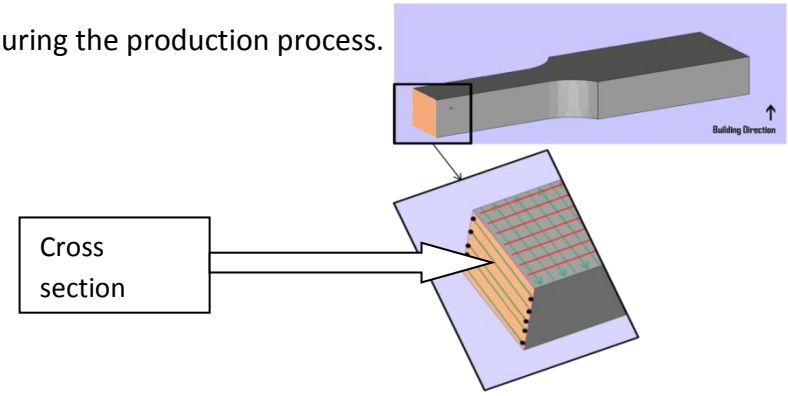

Figure 40 Schematic view of the cross section of XY oriented parts[KEM12]

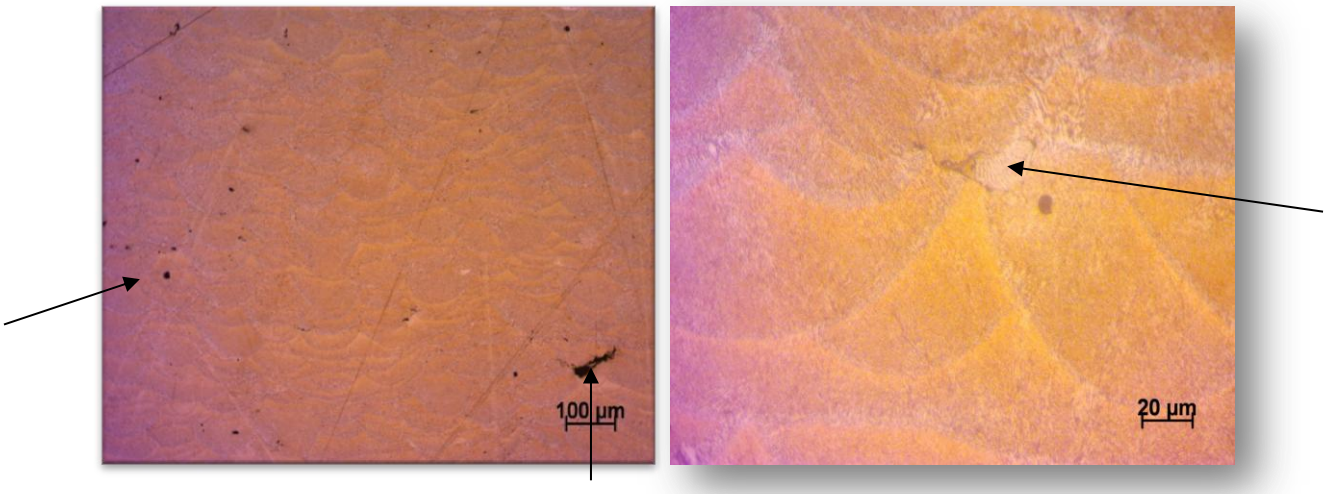

Figure 41 . Microstructure of AlSi10Mg by SLM. A3 batch cross section heat treated(aged, 170°C, 1 hour°C. Higher magnification can be shown in right image. Some spherical pores and irregular pores can be seen. In the right image, the presence of an oxide is shown.

4.7.1. SEM Analysis. Microstructure of C1 part.

With SEM the microstructure and the different zones inside the melt pools were analyzed for one sample of C1 batch. Also, some pores and oxides were analyzed with more detail than in the optical microscope analysis.

C1 part no heat treated (XY oriented, 0°rotation,) was studied in SEM. The top view and the cross section orientation view were analyzed.

4.7.1.1. Top view C1

In the following picture (Figure 44) the tracks are clearly visible. With more magnification in the point A, one can see the different zones, indicated in Figure 43 with more detail. Those are coarse melt pool, fine melt pool and the heat affected zone produced by the laser beam.

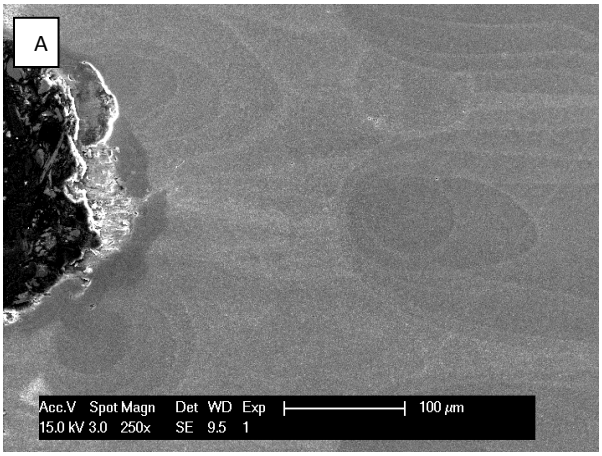

Figure 42 Microstructure of AlSi10Mg by SLM. Top view of XY 0°nHT.

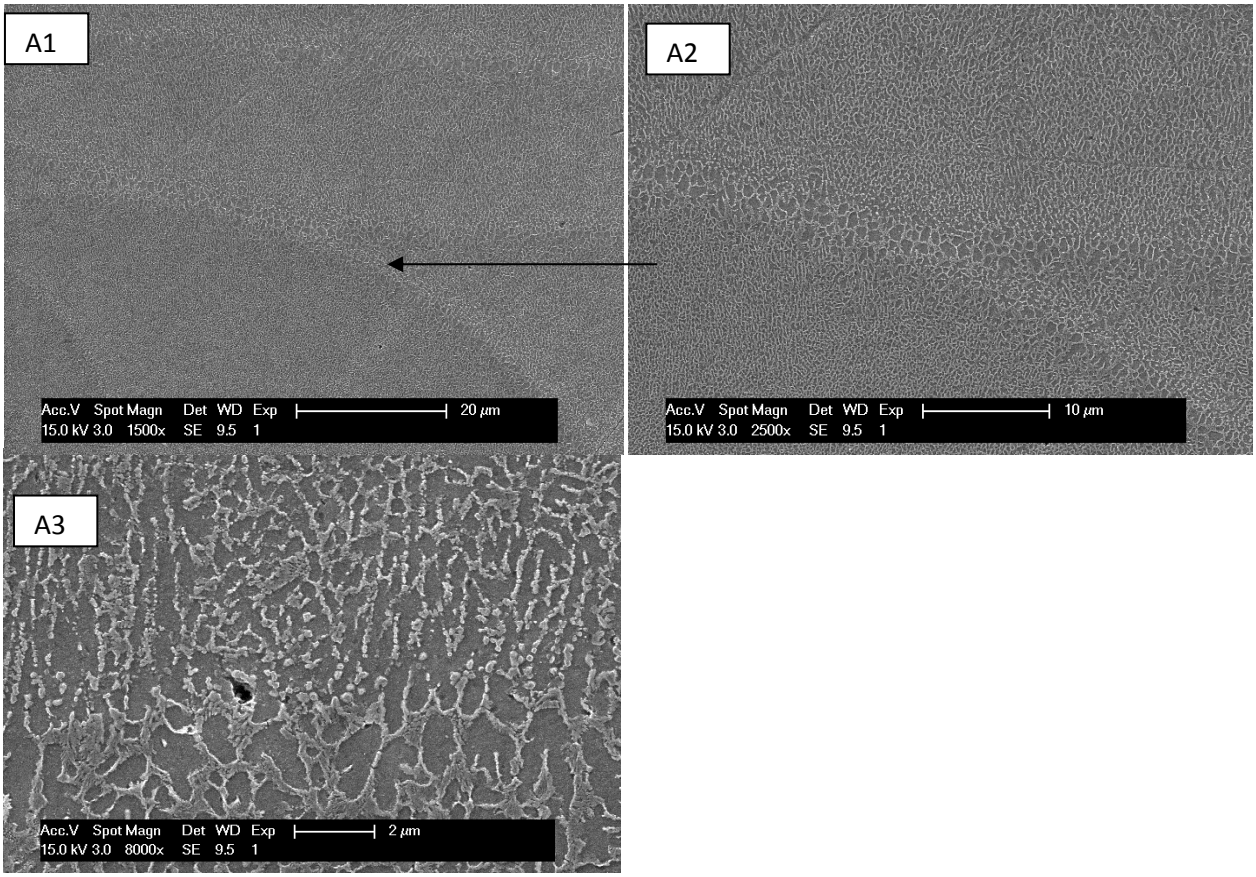

Figure 43 . Microstructure of AlSi10Mg by SLM. Higher magnifications of the A zone.(A1,A2,A3). The coarse and the fine melt pool zones can be distinguished in A2. In A3 one can observe the Heat affected zone(HAZ) indicated by the arrow.

In the following picture one can see the three zones differentiated: Coarse Melt pool (2), fine melt pool (3), and Heat Affected Zone.(1)

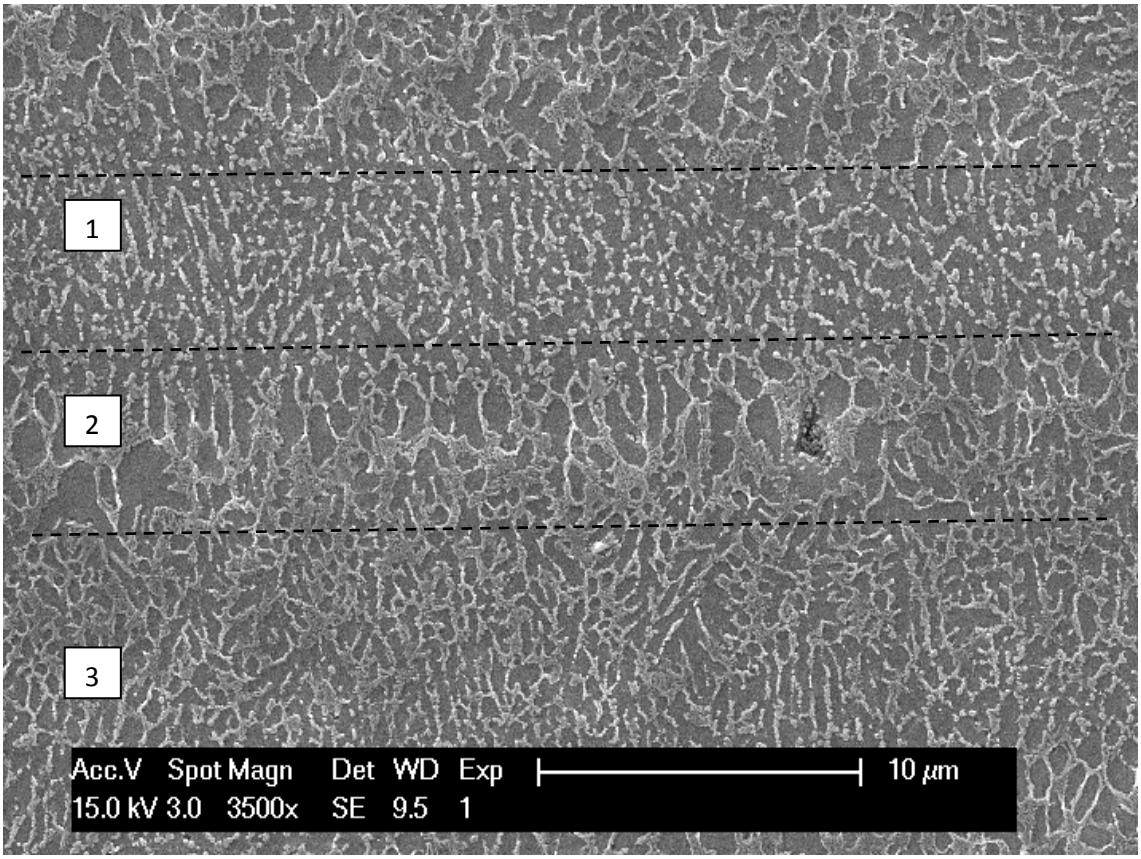

Figure 44. Microstructure of AlSi10Mg by SLM. MP fine(3), MP coarse(2) and HAZ(3).

By S.E.M the characteristically eutectic phase form of Al-Si can be observed. Grey pixels colors correspond to Si, while the α-Al matrix phase appears as a brighter phase.

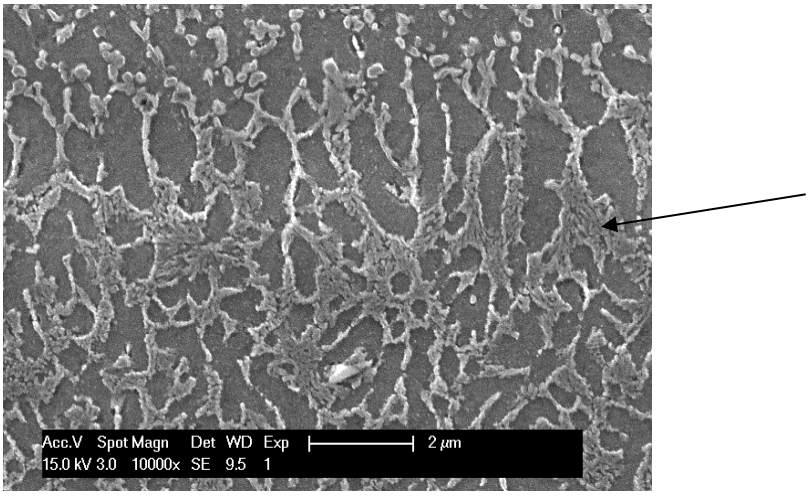

Figure 45 Microstructure of AlSi10Mg by SLM. The arrow shows the eutectic phase of Al-Si.

Some pores and oxides were studied during the analysis. In Figure 46 the XRD patterns reveal an oxide, with peaks corresponding to oxygen, aluminum. The presence of pores can be seen in the right image indicated with an arrow.

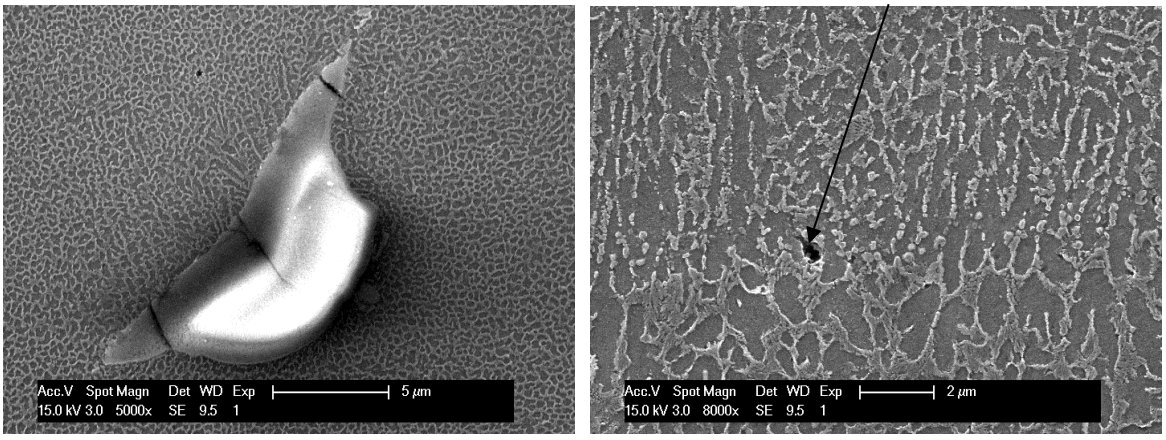

Figure 46. Microstructure of AlSi10Mg by SLM. Presence of oxides (left image) and pores(right image, indicated with an arrow) are revealed in the top view.

4.7.1.2. Cross section view of C1

In the cross section view the orientation of the dentrites can be observed, as well as the melt pool boundaries, and the half pipe form of the melt pool created by the laser beam. Some pores can be seen . InFigure 48 (left), one can see a big pore partially filled with material when polishing. In Figure 48(right) the presence of Titanium and Niquel was revealed by XRD patterns, possibly due to contamination when the powders were produced.

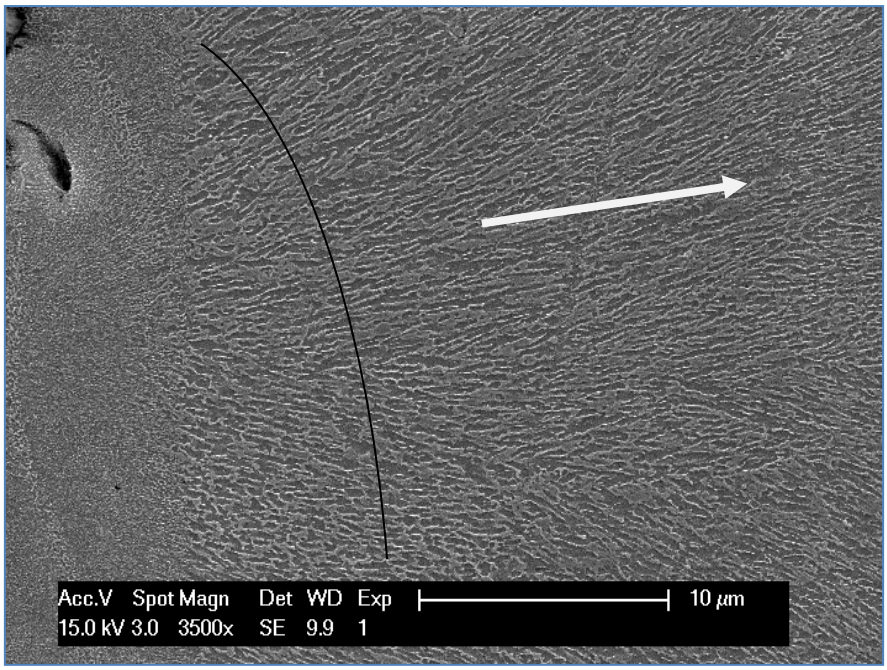

Figure 47 Microstructure of AlSi10Mg by SLM. The orientation of the dentrites can be observed in the cross section view.(arrows) Also the half pipe form of the laser is shown here.(arc)

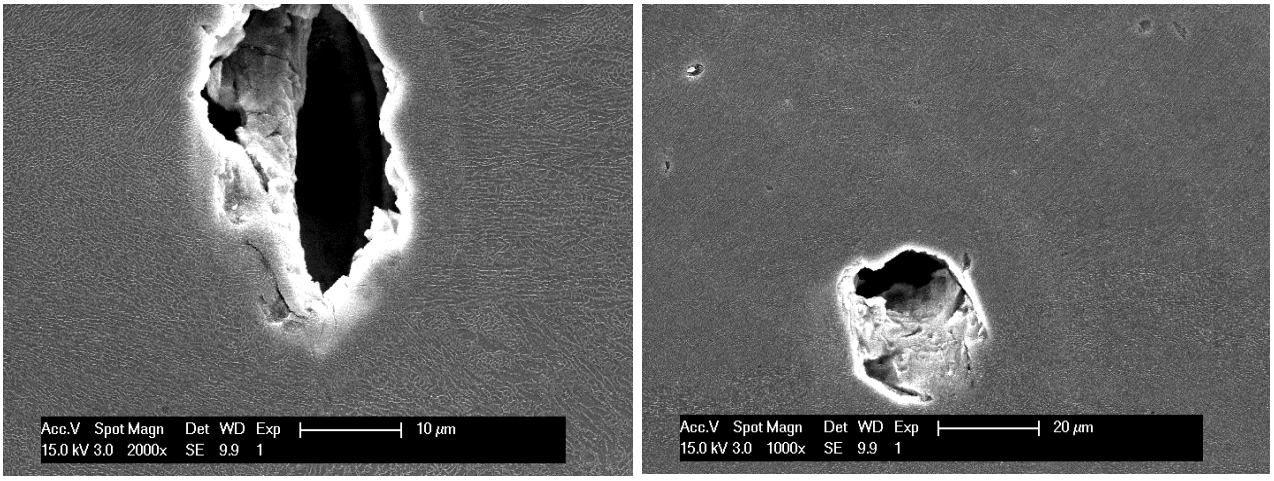

Figure 48 . Microstructure of AlSi10Mg by SLM. Some pores are shown. The XRD pattern revealed the presence of Ti and Ni in the clear zones.

5. Conclusions

- The relative density of the parts of AlSi10Mg studied in this thesis shows a relation with the laser power used to manufacture them. When the laser power is increased, keeping constant the scan speed, one can observe a decrease in the relative density (%) of the parts, which is an indicator of the presence of more porosity in the parts.
- The results also show that there is anisotropy between the XY, XZ and Z building oriented parts. For Z building orientation, where tracks are shorter, the parts show lower elongation to failure. The turbulences in the heat flow contribute to increase the porosity, and keyholes are very sensitive to heat flow variations so can easily form pores that could cause fracture. Also, some borderlines of pores were shown at the beginning and the end of the tracks of the parts (Figure 36) which can be the origin of fracture. Furthermore the presence of some spherical and irregular pores and oxides in the different batches was shown, as well as the microstructure of the melt pool produced by the laser. The melt pool (coarse, fine), and the heat affected zone by the laser were analyzed.
- Related with the scanning strategy, one can see that there is difference in texture depending on the scanning strategy applied. For the parts that were done without rotation, there is a <100> growth of grains in that crystal direction, which correspond to the scanning direction, while for 90°rotated part the crystal orientation in the scanning and building direction is not so definite.
- The mechanical tests show that the mechanical properties of the as produced AlSi10Mg SLM parts are better than the mechanical properties of die casting +aged parts The yield strength, the elongation to failure and the UTS have higher values for the SLM batches studied here than the casted +aged ones, while the E-modulus is similar.

- The aging (175°C, 1 hour) that was done to half of the parts shows that there is a slightly increase in the HV of the SLM parts that were aged. However, the difference is not significant. All the SLM parts studied here (aged and non aged) show higher HV values than the die casting +aged parts. The XY oriented parts show higher hardness than the Z oriented. One cannot see a difference in the rest of mechanical properties neither in microstructure between SLM parts aged and not aged.

6. References

[ASM92] ASM International. ASM Handbook, vol 2; Materials Park, OH; 1992

[BRA12] Erhard Brandl E, HeckenbergerU, Holzinger V ,Buchbinder D. Additive manufactured AlSi10Mg samples using Selective Laser Melting (SLM): Microstructure, high cycle fatigue, and fracture behavior Materials and Design 34 159–169 2012

[VER09] Verhaeghe F, Craeghs T, Heulens J, Pandelaers L. Acta Mater ; 57(20): 6006–12. 2009

[Adial.fr] Web-based data. Adial. <http://www.adial.fr/> [as on 05.04.13]

[TOT03].Totten,George E. Handbook of Aluminium, vol 2. Marcel Dekker,Inc. ; 2003.

[KAY09] Web-based data Kayepresteigne http://www.kayepresteigne.co.uk/tolerance.htm [as on 20.04.13]

[KEM12] Kempen K,Thijs L, Van Humbeeck J and Kruth J-P. Mechanical properties of AlSi10Mg produced by Selective Laser Melting; Physics Procedia Volume 39, 439–446 2012.

[KEM11] Kempen K, Thijs L, Yasa E, Badrossamay M, Verheecke W, Kruth J.; In: Paper presented at the Solid Freeform Symposium (SFF2011),Austin(Texas). 2011

[THI12] Thijs L Kempen K, Kruth J-P ,Van Humbeeck J Fine- structured aluminium products with controllable texture by Selective Laser Melting of pre-alloyed AlSi10Mg powder. Acta Materialia 61 1809-1819 2013

[BOH11] Bohórquez C. A, Sierra Cetina M, Lemus J, Influence of aging heat treatment on the mechanical properties of aluminum 6061 T6 and 6063 T5 AVANCES Investigación en Ingeniería 13 2010

[ZHA01]. Pore Formation during Laser Beam Welding of Die-Cast Magnesium Alloy AM60B — Mechanism and Remedy Zhao H; Debroy T. Welding Research Supplement 209-s 2001.

[KUL13] Web-based data. Description of the devices. http://www.mtm.kuleuven.be/English/Research/Equipment/List as on [20.03.13]

Resumen en castellano:

Las 10 siguientes páginas constituyen una adaptación al castellano de los siguientes apartados del PFC: 1)Abstract, 3)Experimental Procedure y 5)Conclusions.

1. Abstract

Fusión selectiva por láser (SLM) es una técnica de fabricación aditiva que permite la producción de piezas a partir de polvo, utilizando un haz de láser y la ayuda de técnicas CAD de ordenador. Con este sistema se pueden producir piezas geométricas complejas con muy buenas tolerancias dimensionales y piezas de alta calidad y de altas propiedades mecanicas.

El objetivo de esta tesis es el estudio de la microestructura y las propiedades mecánicas de las piezas producidas por AlSi10Mg en función de los parámetros de análisis de SLM y la influencia de los tratamientos de envejecimiento. Por otra parte,se ha realizado una comparación entre las partes tradicionales de colada y piezas de SLM. Para el estudio de las propiedades, se han desarrollado diferentes análisis de microestructura, mediciones de densidad, pruebas de tensión, pruebas de dureza, pruebas de difracción de rayos X y SEM . Además, se analizarán los efectos de un tratamiento de envejecimiento en las partes AlSi10mg.

3. Procedimiento experimental

En este capítulo se describen los diferentes experimentos realizados, explicando los procedimientos y parámetros utilizados en cada una de ellas y las principales características de los dispositivos.

Para el análisis de las piezas de SLM se realizaron los siguientes pasos:

- Las mediciones de densidad
- Tratamiento de Envejecimiento (la mitad de las piezas)
- Ensayo de tracción
- El análisis óptico de la microestructura
- Ensayo de dureza
- SEM (microscopio electrónico de barrido)
- DRX (difracción de rayos X)

a. Medida de la densidad de la aleación utilizada.

Las mediciones de densidad se realizan con el fin de disponer de información sobre la densidad absoluta de las partes. Además, se puede obtener la densidad relativa (%) de las partes, a través de una comparación entre el valor de la densidad teórica de la aleación y el valor medido. La densidad relativa proporciona información sobre la porosidad de las muestras. Para las aleaciones de AlSi10mg, el valor teórico de la densidad es de 2, 68 g/cm3

Para la medición de la densidad, se utiliza el método de Arquímedes. Las muestras se miden en etanol y en el aire. Previamente, la densidad de etanol debe comprobarse, ya que las variaciones de la temperatura o la composición pueden dar valores diferentes.

Así, con una fórmula simple, (1) se puede calcular la densidad absoluta de cada parte.

$$\rho_{abs} = \frac{m_{air} \cdot (\rho_{ethanol} - 0.0012)}{0.999836 \cdot (m_{air} - m_{summerged})} + 0.0012 \quad (1)$$

Donde:

m_{air}= peso de las piezas en aire(g)

$m_{submerged}$= peso de las piezas en etanol (g)

0.0012 g/cm^3=Densidad de Archimedes del aire.

Para obtener la densidad relative de cada pieza la siguiente formula fue usada: (2)

$$\rho_{rel}(\%) = \frac{\rho_{abs}}{\rho_{theoretical}} \cdot 100 \qquad (2)$$

Es importante tener en cuenta que a veces las burbujas de aire atrapadas en el interior de las partes o en las superficies puede dar lugar a una variación en la medición, por lo que es necesario esperar hasta que la pesa indicada se estabiliza.

b. Tratamiento de envejecimiento

Aproximadamente la mitad de las piezas de cada lote fue envejecida . El envejecimiento fue de una hora a 175 ° C , y luego las muestras fueron enfriadas con la puerta del horno cerrada hasta 70 ° C. Después fueron refrigerados por aire . Se utilizó el horno de resistencia de aire 323. Para las mediciones , termopares blindados más un tipo adicional del termopar K fue utilizado , así como un aparato registrador de datos con el fin de visualizar y registrar la temperatura en el horno . Todas las piezas fueron envejecidas con los mismos ajustes y las mismas condiciones en el horno. La figura 5 muestra la evolución de la temperatura en tiempo real . Las muestras se colocaron dentro de la cámara con la misma separación entre ellas y colocadas lateralmente de canto , para permitir la distribución de calor más uniforme posible.

El envejecimiento permite la difusión de átomos que después se precipitan fuera de la solución , como una fase de refuerzo . Por lo tanto cabe esperar un aumento en la dureza debido a la precipitación de elementos intermetalicos en la matriz . El alargamiento y el resto de propiedades no deben comprometerse demasiado [BOH11]

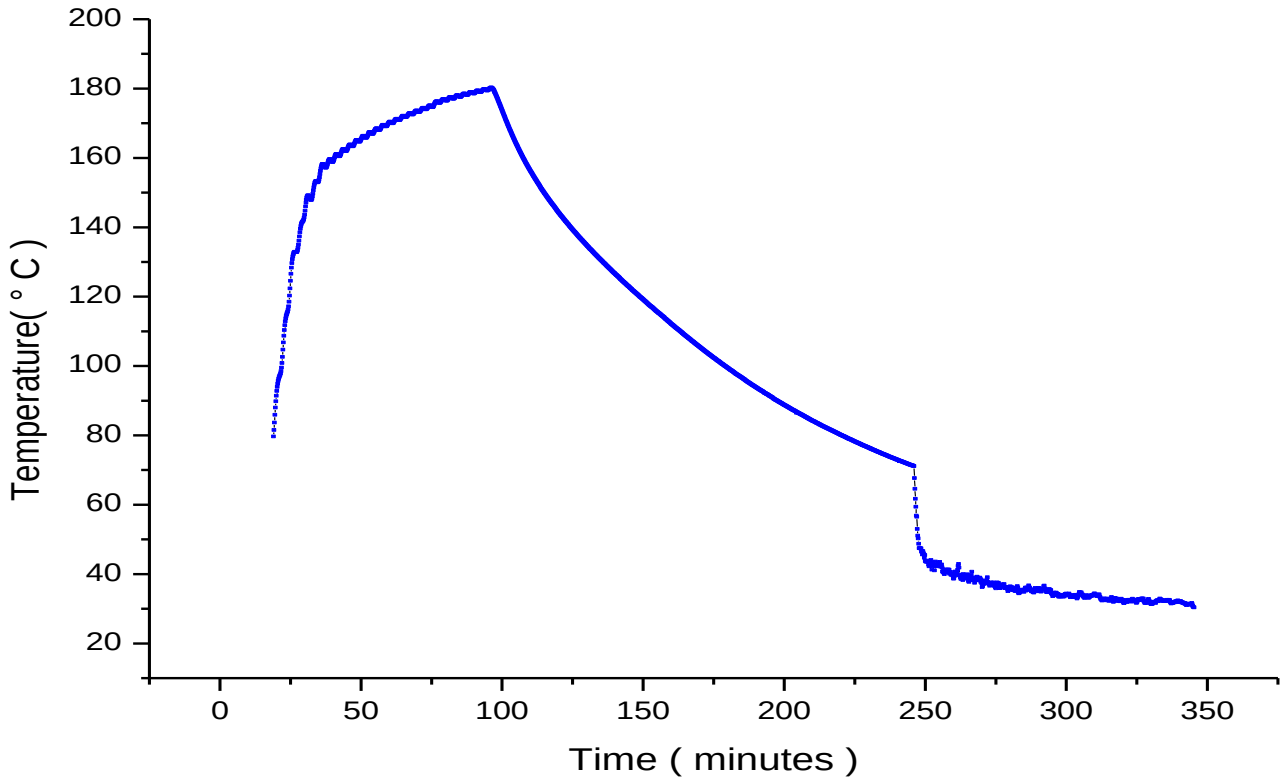

Figure 49 Variación de la temperatura para las piezas de AlSi10Mg (1 hora, 175°C)

c. Test de tracción

Los ensayos de tracción se realizaron en la máquina INSTRON 4505. La velocidad de deformación utilizada fue de 1 mm / min, y la longitud del extensómetro utilizada fue de 12, 5 mm con el fin de tener una medida precisa de la deformación de la muestra que está siendo estudiada

Por ensayo de tracción, se puede obtener información acerca de módulo E, YTS (resistencia a la tracción de rendimiento), UTS (resistencia máxima a la tracción) y el alargamiento a la fractura. La curva de tensión-deformación de una pieza AlSi10Mg hecha por SLM puede ser representada en la Figura 6.

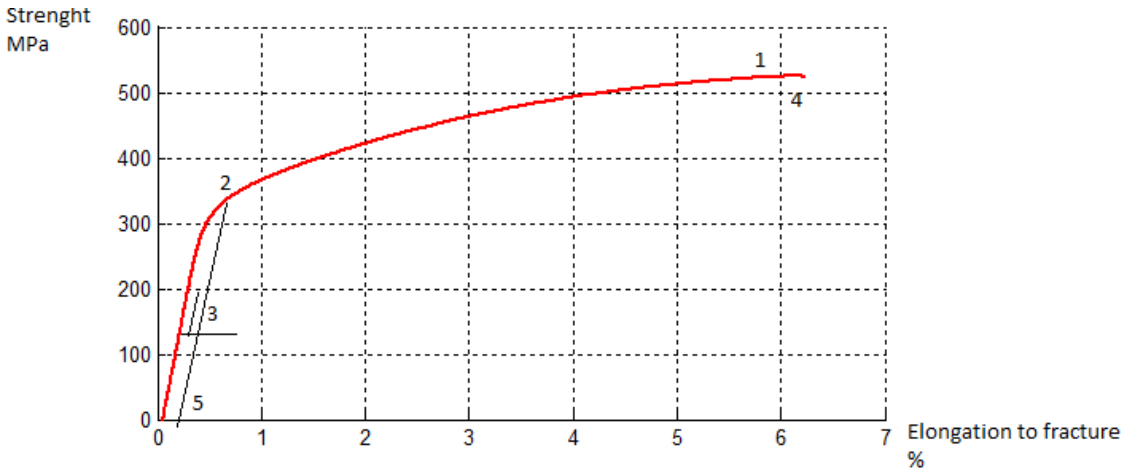

Figure 50 Curva típica de Tensión-Deformación para una pieza de AlSi10Mg.

Los puntos en la figura corresponden a lo siguiente:

1. Resistencia a la tracción (UTS): Es la tensión máxima que el material puede soportar en un ensayo de tracción.

2. Límite elástico (YTS): Es el punto en el que el material comienza a deformarse plásticamente.

3. Módulo de Young: Es la medida de la rigidez en la región elástica del material. Corresponden a la pendiente de la curva en la región elástica

4. Fractura:. El punto representa el alargamiento máximo a la fractura (eje x)

5. Offstress (típicamente 0,2%)

d. Hardness test measurement

El objetivo era medir la dureza de las piezas, tanto en la dirección de construcción como en la dirección del escaner. Esta prueba da una medida de la resistencia contra la deformación. Las medidas se tomaron según la escala de dureza Vickers. Por otra parte, se puede establecer una comparación entre las partes de envejecidas y no envejecidas , y entre las producidas por los mètodos tradicionales y las producidas por SLM, además de estudiar la relación entre los difernetes modos de escaneado y los parámetros usados en cada una de los lotes. El equipo utilizado para la prueba fue FV700B. Los parámetros utilizados son los siguientes:

- Test: VICKERS
- Tiempo de Test: 10s
- Objetivo: X50
- Fuerza en el Test: 0, 3 kg

e. Análisis mediante microscopio óptico

Para el análisis óptico las muestras fueron observadas con un microscopio polarizado Axioskop 40 Pol/40 A Pol. Las lentes ópticas usadas fueron Carl Zeis con los aumentos X4, X10, X50, X100.

Figure 51 Microscopio óptico Axioskop[KUL13]

1. Preparación de las muestras

Para la preparación de las muestras, primero fue necesario cortarlas. Dos recortes de 1cm^2 y un espesor de alrededor de 4 mm fueron hechos en cada muestra, con el fin de obtener una vista desde arriba en la dirección de escaneado y una sección transversal vista orientada en la dirección edificio. Un polímero se utiliza para incrustar las piezas. Para la parte que fue escaneada el SEM, se utilizó resina fenólica con relleno de carbono. Al usar este polímero termoestable con el carbono, la muestra se convierte en conductora , lo cual es indispensable para el análisis SEM. Después de eso, las partes se lijan y se pulen.

Figure 52 Crimping, (a) lijado (b) y pulido (c).

2. Atacantes

Los reactivos de ataque utilizados para las partes fueron HF , el reactivo de Keller y reactivo de Barker

El reactivo de Keller se utiliza para aluminio y aleaciones de aluminio . Funciona bien para revelar los límites de grano . Se basa en una mezcla de HF , HCl y HNO3 con agua . (Mezclado como 1,0 ml de HF y HCl 1,5 ml en 2,5 ml de HNO3 y 95 ml de agua) . El reactivo Barker ' s fue efectivo para visualizar la microestructura utilizando luz polarizada en la microscopía óptica. Su composición se basa en la mezcla de ácido fluobórico con agua . El tiempo de exposición a los agentes fue un parámetro importante a controlar, con el fin de evitar el sobreataque en las partes.

f . SEM (Scanning Electron Microscope)

La técnica SEM produce imágenes de la muestra utilizando un haz enfocado de electrones , mediante la interacción de ellos con la muestra . El microscopio usado fue un microscopio electrónico de barrido PHILIPS XL30 FEG .

Una pieza (XY 0 ° NHT , sin refusión) fue escaneada con SEM . Con SEM , se puede lograr alta resolución, obteniendo imágenes tan detalladas como los granos en la zona afectada por el calor o imágenes de gran aumento de los poros.

La superficie de la pieza debe ser conductora para los electrones . Para este propósito , el polímero utilizado para prensar la muestra contiene carbono, por lo que la muestra

se convierte en conductora . Luego se aplicó presión con el fin de curar el polímero . De ese modo , una pequeña clase de tratamiento térmico se podría haber producido debido al calor desprendido por la máquina. Pero , teniendo en cuenta el tiempo de exposición tan corto , y la baja temperatura , se puede obviar este tratamiento térmico " no deseado " .

g . Técnicas de difracción de rayos- X . textura

Mediante textura , se puede determinar y estudiar la orientación de los granos de una pieza . Se puede representar mediante una figura polar . Para la medición de cuatro muestras (xy0 ° HT , xy0 ° NHT , Z90 ° NHT y Z0 ° NHT) se utilizó el D500 goniómetro , mediante un tubo de Cu a 40 kV y 40 mA . Las figuras de polo se obtuvieron para (111) , (200) , (220) y (311)

En primer lugar, las muestras se lijaron y pulieron adecuadamente. A continuación, las piezas se introdujeron en el interior del soporte de la máquina. Para cada muestra,se comprobaron primero los picos de difracción. Los resultados se analizaron con el fin de obtener la representación visual de la textura (figura polar)

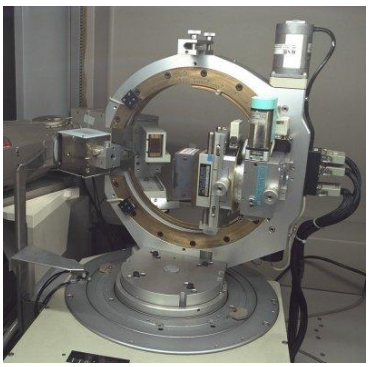

Figure 53 D500 goniometer was used in order to measure the texture of the AlSi10Mg samples. [KUL13]

5. Conclusiones

La densidad relativa de las partes de AlSi10mg estudiada en esta tesis muestra una relación con la potencia del láser utilizado para su fabricación. Cuando se aumenta la potencia del láser , manteniendo constante la velocidad de exploración , se puede observar una disminución en la densidad relativa (%) de las partes , lo cual es un indicador de la presencia de más porosidad en las piezas . Los resultados también muestran que hay anisotropía entre XY , XZ y las partes orientadas en la direccion Z . Para la orientación de Z, donde las pistas son más cortas, las piezas muestran menor alargamiento a la rotura . Las turbulencias en el flujo de calor contribuyen a aumentar la porosidad , y los keyholes son muy sensibles a las variaciones del flujo de calor por lo que se puedne formar fácilmente poros que podrían causar fractura . Además, algunas de las líneas divisorias de los poros que aparecen al inicio y al final de las pistas de las piezas (Figura 36) pueden ser el origen de la fractura . Además, la presencia de algunos poros y óxidos esféricos e irregulares en los diferentes lotes se pueden apreciar, así como la microestructura de la meltpool fundida producida por el láser. Se analizaron la zona de fusion (zonas de grano grueso y fino) , y la zona afectada por el calor por el láser .

En relación con la estrategia de exploración seguida , se puede ver que hay una diferencia en la textura dependiendo de la estrategia de exploración aplicada. Para las partes que se hicieron sin rotación , hay una estructura visible orientada < 100 > que muestra el crecimiento de los granos de cristal en esa dirección, mientras que para la que fue creada con rotación de 90 ° la orientación de los cristales en la exploración y la dirección edificio no es tan definida .

Los ensayos mecánicos muestran que las propiedades mecánicas de las piezas de AlSi10mg producidas por SLM son mejores que las propiedades mecánicas de piezas producidas mediante casting + envecimiento. El límite de elasticidad , la elongación a la fractura y la UTS tienen valores más altos para los lotes SLM

estudiadosaquí que el + casting + envejecimiento, mientras que el módulo de elasticidad es similar .

El envejecimiento (175 ° C , 1 hora) que se hizo para la mitad de las piezas muestra que hay un ligero aumento en el HV de las partes SLM que fueron envejecidas . Sin embargo , la diferencia no es significativa . Todas las partes de SLM estudiados aquí (envejecidas y no) muestran valores más altos que el HV Die Casting + envejecimiento. Las partes orientadas en la dirección XY muestran una mayor dureza que las orientadas en Z . Sin embargo no se puede apreciar una diferencia significativa en el resto de las propiedades mecánicas ni en la microestructura entre las partes de SLM que fueron envejecidas y aquellas que no lo fueron.